Feng ZM, Wu AZ and Chen CL (1995) Characterization and regulation of two testicular inhibin/activin beta B-subunit messenger ribonucleic acids that are transcribed from alternate initiation sites. Endocrinology 136,947–955.

Groome NP, Illingworth PJ, O'Brien M, Cooke I, Ganesan TS, Baird DT and McNeilly (1994) Detection of dimeric inhibin throughout the human menstrual cycle by two-site enzyme immunoassay. Clin Endocrinol 40,717–723.

Groome NP, Illingworth PJ, O'Brien M, Pai R, Rodger FE, Mather JP and McNeilly (1996) Measurement of dimeric inhibin B throughout the human menstrual cycle. J Clin Endocrinol Metab 81,1401–1405.

Hamada H and Kakunaga T (1982) Potential Z-DNA forming sequences are highly dispersed in the human genome. Nature 298,396–398.

Hamada H, Petrino MG and Kakunaga T (1982) A novel repeated element with Z-DNA-forming potential is widely found in evolutionarily diverse eukaryotic genomes. Proc Natl Acad Sci USA 79,6465–6469.

Harris SE, Chand AL, Winship IM, Gersak K, Aittomaki K and Shelling AN (2002) Identification of novel mutations in FOXL2 associated with premature ovarian failure. Mol Hum Reprod 8,729–733.

Hsu SY, Lai RJ, Nanuel D and Hsueh AJ (1995) Different 5′-flanking regions of the inhibin-alpha gene target transgenes to the gonad and adrenal in an age-dependent manner in transgenic mice. Endocrinology 136,5577–5586.

Keelan J, Song Y and France JT (1994) Comparative regulation of inhibin, activin and human chorionic gonadotropin production by placental trophoblast cells in culture. Placenta 15,803–818.

Latronico AC, Anasti J, Arnhold IJ, Rapaport R, Mendonca BB, Bloise W, Castro M, Tsigos C and Chrousos GP (1996) Brief report: testicular and ovarian resistance to luteinizing hormone caused by inactivating mutations of the luteinizing hormone-receptor gene. N Engl J Med 334,507–512.

Ling N, Ying SY, Ueno N, Esch F, Denoroy L and Guillemin R (1985) Isolation and partial characterization of a Mr 32,000 protein with inhibin activity from porcine follicular fluid. Proc Natl Acad Sci USA 82,7217–7221.

Ling N, Ying SY, Ueno N, Shimasaki S, Esch F, Hotta M and Guillemin R (1986) A homodimer of the beta-subunits of inhibin A stimulates the secretion of pituitary follicle stimulating hormone. Biochem Biophys Res Commun 138,1129–1137.

Marozzi A, Porta C, Vegetti W, Crosignani PG, Tibiletti MG, Dalpra L and Ginelli E (2002) Mutation analysis of the inhibin alpha gene in a cohort of Italian women affected by ovarian failure. Hum Reprod 17,1741–1745.

Meunier H, Rivier C, Evans RM and Vale W (1988) Gonadal and extragonadal expression of inhibin alpha, beta A, and beta B subunits in various tissues predicts diverse functions. Proc Natl Acad Sci USA 85,247–251.

Miyamoto K, Hasegawa Y, Fukuda M, Nomura M, Igarashi M, Kangawa K and Matsuo H (1985) Isolation of porcine follicular fluid inhibin of 32K daltons. Biochem Biophys Res Commun 129,396–403.

Montgomery GW, Duffy DL, Hall J, Haddon BR, Kudo M, McGee EA, Palmer JS, Hsueh AJ, Boomsma DI and Martin NG (2000) Dizygotic twinning is not linked to variation at the alpha-inhibin locus on human chromosome 2. J Clin Endocrinol Metab 85,3391–3395.

Nishi Y, Yanase T, Mu Y, Oba K, Ichino I, Saito M, Nomura M, Mukasa C, Okabe T, Goto K et al. (2001) Establishment and characterization of a steroidogenic human granulosa-like tumor cell line, KGN, that expresses functional follicle-stimulating hormone receptor. Endocrinology 142,437–445.

Pei L, Dodson R, Schoderbek WE, Maurer RA and Mayo KE (1991) Regulation of the alpha inhibin gene by cyclic adenosine 3′,5′-monophosphate after transfection into rat granulosa cells. Mol Endocrinol 5,521–534.

Rivier J, Spiess J, McClintock R, Vaughan J and Vale W (1985) Purification and partial characterization of inhibin from porcine follicular fluid. Biochem Biophys Res Commun 133,120–127.

Robertson DM, Foulds LM, Leversha L, Morgan FJ, Hearn MT, Burger HG, Wettenhall RE and de Kretser DM (1985) Isolation of inhibin from bovine follicular fluid. Biochem Biophys Res Commun 126,220–226.

Shelling AN (2000) X chromosome defects and premature ovarian failure. Aust N Z J Med 30,5–7.

Shelling AN, Burton KA, Chand AL, van Ee CC, France JT, Farquhar CM, Milsom SR, Love DR, Gersak K, Aittomaki K et al. (2000) Inhibin: a candidate gene for premature ovarian failure. Hum Reprod 15,2644–2649.

Su JG and Hsueh AJ (1992) Characterization of mouse inhibin alpha gene and its promoter. Biochem Biophys Res Commun 186,293–300.

Tanimoto K, Yoshida E, Mita S, Nibu Y, Murakami K and Fukamizu A (1996) Human activin betaA gene. Identification of novel 5′ exon, functional promoter, and enhancers. J Biol Chem 271,32760–32769.

Touraine P, Beau I, Gougeon A, Meduri G, Desroches A, Pichard C, Detoeuf M, Paniel B, Prieur M, Zorn JR et al. (1999) New natural inactivating mutations of the follicle-stimulating hormone receptor: correlations between receptor function and phenotype. Mol Endocrinol 13,1844–1854.

Vale W, Rivier C, Hsueh A, Campen C, Meunier H, Bicsak T, Vaughan J, Corrigan A, Bardin W, Sawchenko P et al. (1988) Chemical and biological characterization of the inhibin family of protein hormones. Recent Prog Horm Res 44,1–34.

Vale W, Rivier J, Vaughan J, McClintock R, Corrigan A, Woo W, Karr D and Spiess J (1986) Purification and characterization of an FSH releasing protein from porcine ovarian follicular fluid. Nature 321,776–779.

Yoshida E, Tanimoto K, Murakami K and Fukamizu A (1998) Isolation and characterization of 5′-regulatory region of mouse activin beta A subunit gene. Biochem Mol Biol Int 44,325–332.

Submitted on June 21, 2005; accepted on July 26, 2005

Available online at www.sciencedirect.com

SCIENCE DIRECT

Biochimica et Biophysica Acta 1728 (2005) 84–94

BIOCHIMICA ET BIOPHYSICA ACTA
BBA

http://www.elsevier.com/locate/bba

Dehydroepiandrosterone negatively regulates the p38 mitogen-activated protein kinase pathway by a novel mitogen-activated protein kinase phosphatase

Kenji Ashida, Kiminobu Goto, Yue Zhao, Taijiro Okabe, Toshihiko Yanase, Ryoichi Takayanagi, Masatoshi Nomura, Hajime Nawata*

Department of Medicine and Bioregulatory Science (3rd Department of Internal Medicine), Graduate School of Medical Sciences, Kyushu University, Maidashi 3-1-1, Higashi-ku, Fukuoka 812-8582, Japan

Received 10 May 2004; received in revised form 10 January 2005; accepted 26 January 2005

Abstract

Dehydroepiandrosterone-sulfate, the sulfated form of dehydroepiandrosterone, is the most abundant steroid in young adults, but gradually declines with aging. In humans, the clinical application of dehydroepiandrosterone targeting some collagen diseases, such as systemic lupus erythematosus, as an adjunctive treatment has been applied in clinical trial. Here, we report that dehydroepiandrosterone may negatively regulate the mitogen-activated protein kinase pathway in humans via a novel dual specificity protein phosphatase, DDSP (dehydroepiandrosterone-enhanced dual specificity protein phosphatase). DDSP is highly homologous to LCPTP/HePTP, a tissue-specific protein tyrosine phosphatase (PTP) which negatively regulates both ERK and p38-mitogen-activated protein kinase, and is transcribed from the PTPN7 locus by alternative splicing. Although previous reports have shown that the mRNA expression of the LCPTP/HePTP gene was inducible by extracellular signals such as T-cell antigen receptor stimulation, reverse transcribed (RT)-PCR experiments using specific sets of primers suggested that the expression of LCPTP/HePTP was constitutive while the actual inducible sequence was that of DDSP. Furthermore DDSP was widely distributed among different types of human tissues and specifically interacted with p38-mitogen-activated protein kinase. This inducible negative regulation of the p38-mitogen-activated protein kinase-dependent pathway may help to clarify the broad range of dehydroepiandrosterone actions, thereby aiding the development of new preventive or adjunctive applications for human diseases.

Keywords: Dehydroepiandrosterone; Dual specificity protein phosphatase; Protein tyrosine phosphatase; p38-mitogen-activated protein kinase; Mitogen-activated protein kinase; Mitogen-activated protein kinase phosphatase

1. Introduction

The mitogen-activated protein kinase (MAPK) family plays a central role in signaling pathways stimulated by extracellular stimuli such as growth factors, cytokines and physical stress. In higher organisms, this kinase family includes the extracellular stimulus-regulated kinases (ERKs) and two stress-stimulated kinase groups, the stress-activated protein kinase/c-JUN N-terminus kinase (SAPK/JNK) and p38-MAPK/p38 High Osmolarity Glycerol response (HOG) 1 [1–5]. The activation of MAPKs requires phosphorylation of conserved tyrosine and threonine residues within the catalytic domain. This phosphorylation is mediated by dual

Abbreviations: RT-PCR, reverse transcribed PCR; MAPK, mitogen-activated protein kinase; PTP, protein tyrosine phosphatase; DSP, protein dual specificity phosphatase; LCPTP, leukocyte-specific protein tyrosine phosphatase; HePTP, hematopoietic tissue-specific protein tyrosine phosphatase; DHEA, dehydroepiandrosterone; DDSP, dehydroepiandrosterone-induced protein dual specificity phosphatase; ERK, extracellular stimulus-regulated kinase; JNK, c-*Jun* N-terminus kinase; TcR, T-cell antigen receptor; GFP, green fluorescence protein; PMA, phorbol-12-myristate-13-acetate; aa, amino acid; SSH, suppression subtraction hybridization

* Corresponding author. Tel.: +81 92 642 5275; fax: +81 92 642 5297.
E-mail address: nawata@intmed3.med.kyushu-u.ac.jp (H. Nawata).

0167-4781/$ - see front matter © 2005 Elsevier B.V. All rights reserved.
doi:10.1016/j.bbaexp.2005.01.016

specificity protein kinases, members of the MAPK kinase family. In contrast, in the absence of a signal the constituents of the MAPK cascade return to their inactive dephosphorylated state, suggesting an essential role for protein phosphatases in the negative regulation of the MAPK cascade. Protein phosphatases are classified into three groups, protein serine/threonine phosphatases, protein tyrosine phosphatases (PTPs) and protein dual specificity serine/threonine/tyrosine phosphatases (DSPs), depending on their phosphoamino acid specificity [6].

Dehydroepiandrosterone-sulfate (DHEA-S), the sulfated form of DHEA, is the most abundant steroids in young adults, but gradually decline with aging. Although the molecular basis of DHEA action still remains to be elucidated, recent findings have suggested modulatory actions of DHEA on the MAPK signal transduction pathway [7–9]. To date, much data have been accumulated on the biological action of DHEA, although some of these were carried out using rodents in which the P450 C17 activities are extremely low, thus leading to trace or nearly undetectable levels of serum DHEA or DHEAS concentrations. In humans, the clinical application of DHEA targeting hormone replacement therapy [10–13] has been tested in clinical trials.

We have been interested in the actions of DHEA using both in vitro and in vivo experiments [14] (for review). We have previously reported that a human clonal T lymphocyte, the PEER cell [15], which is stimulated with phorbol-12-myristate-13-acetate (PMA) and calcium ionophore A23187 to mimic the activation of the T-cell antigen receptor (TcR), revealed the specific binding of [3H]-DHEA to its putative receptor. This specific binding was further increased when treated with 100 nM of DHEA itself in addition to the PMA and A23187 treatment [16], while the subcellular localization of the DHEA-bound molecule(s) was not determined. In the experiment, the MAPK cascade was activated by PMA, which bypasses all receptor-induced proximal tyrosine phosphorylation events by directly activating the Raf kinase through protein kinase C [17,18]. Thus, PEER cells are likely to provide a good model for investigating the cellular phenotypes altered by the DHEA action on the MAPK cascade, or for identifying the putative receptor for DHEA. Here, we report that DHEA negatively regulates the MAPK pathway in humans via a novel MAPK phosphatase, tentatively named DDSP (DHEA-enhanced DSP), which is highly homologous to LCPTP/HePTP [19,20] not only controlling the activity of MAPKs but also mediating crosstalk between the cAMP system and the MAPK cascade [21].

2. Materials and methods

2.1. Cells

Human T lymphoblastic leukemic cells, PEER, were maintained in RPMI 1640 (Gibco) supplemented with 10% FBS, 60 μg/ml of benzylpenicillin, 100 μg/ml of streptomycin, 2 mmol/L of L-glutamine, and 50 μmol/L of 2-mercaptoethanol. The cells were plated at a concentration of 1×10^5/ml and then treated with 5 nM PMA and 500 ng/ml of calcium ionophore A23187 in the presence or absence of 50 to 100 nM of DHEA (PEER(+) and PEER(−), respectively) for 28 h. NIH3T3 mouse fibroblasts were maintained in DMEM (Gibco) supplemented with 10% FBS, 60 μg/ml of benzylpenicillin, 100 μg/ml of streptomycin, and 2 mmol/L of L-glutamine.

2.2. Suppression subtractive hybridization screening and reverse transcribed-PCR (RT-PCR)

Total RNA was isolated using ISOGEN (Nippon Gene Co.). Suppression subtraction hybridization (SSH) was performed to construct a subtraction cDNA library using a commercially available kit (PCR-Select cDNA Subtraction Kit, Clonetech Laboratories Inc.). Briefly, double-stranded cDNAs were synthesized using the poly(A)$^+$RNAs from PEER(+) or PEER(−) cells. After the completion of two rounds of hybridization, the suppression PCR products were amplified using the GeneAmp 9600 PCR System (Perkin Elmer Applied Biosystems Division), size-fractionated using Chroma Spin+TE-200 Columns (Clontech Laboratories Inc.) and then blunt ligated into pBluescript II SK—which was cleaved with *Sma*I. DH5α was transformed with the ligation mixtures to construct the plasmid library without amplification.

The nucleotide sequences of 400 randomly chosen clones were determined using a DSQ-1000 DNA Sequencer (Shimadzu Co) and subjected to a homology search. PCR primers of 16-mers specific for the nucleotide sequence of each clone were synthesized and used for RT-PCR to confirm the effect of the DHEA treatment. Semiquantitative RT-PCR was performed using total RNAs from untreated PEER cells, PEER(+) and PEER(−) cells. The PCR fragments were electrophoresed in a 4% polyacrylamide gel. The gels were stained with Cyber Green (Amersham Life Science) and the intensities of the fluorescent signals were analyzed directly using a STORM 860 Image Analyzer (Molecular Dynamics Inc.). A phage cDNA library using the mRNAs from PEER (+) cells was constructed using a ZAP-cDNA Synthesis Kit (Stratagene) and then probed with a clone 1–20 cDNA insert. Thereafter, 1×10^6 plaques were subjected to screening.

2.3. Phosphatase assay

The full-length cDNA sequence of DDSP was ligated into the pAcGHLT baculovirus expression vector (Pharmingen), containing a 6× histidine tag and a glutathione *S*-transferase (GST) tag upstream of the multiple cloning sites, and then transfected into SF-9 (*Spodoptera frugiperda* pupal ovary) insect cells using the calcium phosphate precipitation method. Cells were grown at 25 °C and the viruses were enriched according to the manufacturer's protocol. The expressed GST-DDSP protein was purified using a glutathione sepharose affinity column. Phosphatase assays were performed using the Tyrosine Phosphatase Assay System and the Serine/Threonine Phosphatase Assay System (Promega Co.).

2.4. Tissue distribution and hormonal regulation of DDSP mRNA

The tissue distribution and hormonal regulation of DDSP or LCPTP/HePTP mRNA were examined by semiquantitative RT-

PCR. To compare the tissue distribution and steroid hormone-specific mRNA induction between DDSP and LCPTP/HePTP, 2 sets of primers were designed (Fig. 1), namely one for amplifying the sequences specific to DDSP (5′-GGA-TATTGTGTGCCAACTGC-3′ for the forward and 5′-GAGA-CAGGGTTTACACCATG-3′ for the reverse) and the other for amplifying the sequences specific to LCPTP/HePTP (5′-CAGCTGCTTCAGCAGACCTC-3′ for the forward and 5′-

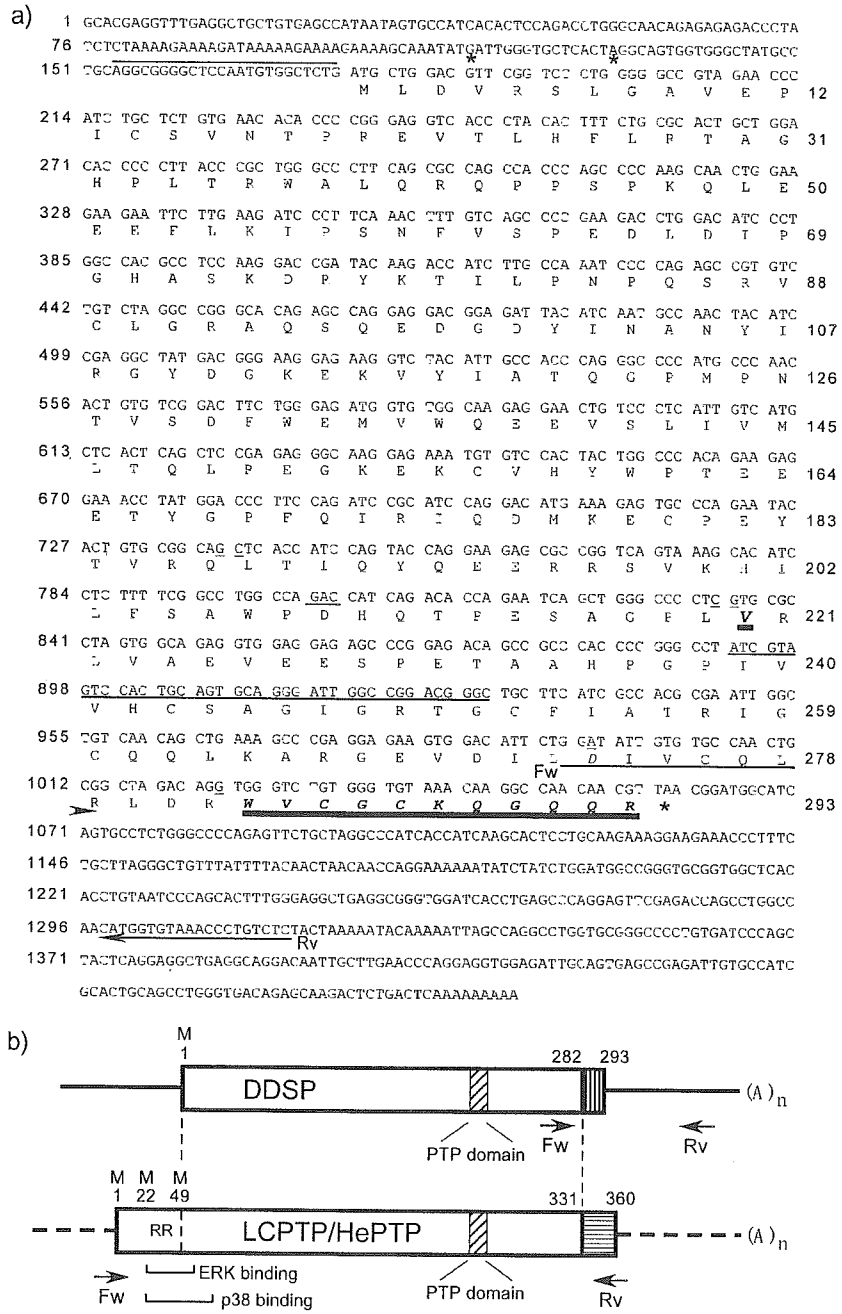

Fig. 1. The structure of DDSP. (a) The nucleotide and aa sequence of DDSP. The nucleotide number and the aa residue number are shown on the left side and right side, respectively. The substitution of the LCPTP/HePTP amino acid residues with the DDSP specific residues are highlighted by italic letters and bold lines, and the 2 termination codons are shown by asterisks. The putative PTP/DSP catalytic domain and Asp209, which is thought to be critical for PTP/DSP activity, are underlined. Arrows labeled with Fw and Rv are forward (Fw) and reverse (Rv) primers, respectively. (b) Schematic comparison of the DDSP structure with the LCPTP/HePTP structure. In DDSP, the aa residues required for ERK binding (including Arg41 and Arg42 shown as "RR" in the figure) are lacking (see text). The C-terminal 11 aa residues of DDSP (vertical bars) are different from those of LCPTP/HePTP (horizontal bars). The dashed box represents the PTP/DSP central catalytic domain. Arrows labeled with Fw and Rv are forward (Fw) and reverse (Rv) primers, respectively.

GGGGCTGGGTTCCTCAGGCA-3′ for the reverse). Tissue cDNA panels (Clontech Laboratories Inc.) were used for the RT-PCR.

2.5. Subcellular localization of DDSP

The full length DDSP cDNA sequence was ligated in-frame into pEGFP (Clontech), thus generating pDDSP-GFP in which the C′-terminus of the DDSP sequence was fused to the N′-terminus of green fluorescence protein (GFP). pDDSP-GFP was transfected into COS-7 cells and the cells were observed using a Leica TCS-SP System confocal laser microscope (Leica Microsystems). The cells were imaged for green fluorescence by excitation with the 488 nm line from an argon laser and the emission was viewed through a 496 to 505 nm band pass filter.

2.6. Immunocoprecipitation and Western blot analysis

For the immunocoprecipitation experiments, NIH3T3 mouse fibroblasts were transfected with a plasmid expressing flag-tagged DDSP using Superfect (Qiagen). At 24 h posttransfection, the cells were stimulated with 0.5 M NaCl for 20 min (for p38- and JNK-MAPK) or 50 ng/ml of PMA for 15 min after incubation in a serum free medium for 15 h (for ERK). Whole cell lysates were prepared by lysing the cells in a buffer (1.0% Nonidet P-40, 50 mM Tris–HCl pH 7.8, 150 mM NaCl, 1 mM DTT, 1 tablet of a protease inhibitor cocktail (Roche)). The lysates were incubated at 4 °C for 1 h with antibodies against ERK, JNK- or p38-MAPK (Cell Signaling) in an immunoprecipitation buffer (0.5% Nonidet P-40, 1 mM EDTA, 50 mM Tris–HCl pH 7.8, 200 mM NaCl, 1 mM DTT, 1 tablet of the protease inhibitor cocktail), and then further incubated with protein-A sepharose beads (Pharmacia) at 4 °C for 2 h. For Western blotting, the samples were separated by SDS-PAGE, transferred to a nitrocellulose filter, and then probed with an antibody against flag according to the manufacturer's protocol. To test the inactivation of the MAPK pathway by DDSP, two sets of transfection experiments were performed. In one experiment, the flag-tagged DDSP cDNA was transfected into NIH3T3 cells, and the transfected cells were then treated to activate ERK, p38 or JNK-MAPKs as in the immunocoprecipitation experiments. The transfection efficiency was monitored by the transfection of pEGFP in a separate dish and resulted in 30 to 50% efficiency. Western blotting was performed to observe the dephosphorylation of endogenous MAPK in the whole cell lysates of transfected cells using anti-phospho-MAPK antibodies (Cell Signaling). To observe the dephosphorylation of the endogenous activated MAPKs, the MACSelect system (Miltenyi Biotech) was used to enrich the transfected cells. The flag-tagged DDSP cDNA was ligated into the pMACSK^{k}II vector plasmid to generate pMACS-DDSP and the NIH3T3 cells were transfected in a 10 cm dish with 20 μg of pMACS-DDSP, or pMACSK^{k}II as a control. The transfected cells were subjected to affinity-column separation and then treated with 0.4 M sorbitol for 20 min to activate p38-MAPK, or 50 ng/ml of PMA for 15 min after incubation in a serum free medium for 20 h for ERK. Nearly 80% of the recovered cells were revealed to be transfected when the efficiency was preliminarily monitored by the cotransfection of pMACSK^{k}II and pEGFP. Western blotting was performed using anti-phospho-p38 or -ERK antibodies (Cell Signaling).

3. Results

3.1. Isolation of a cDNA sequence homologous to LCPTP/HePTP

Human T-cell leukemia cells (PEER) were treated with PMA and calcium ionophore A23187 to mimic TcR activation with (PEER(+)) or without (PEER(−)) 50 nM of DHEA. We performed the SSH screening by constructing a cDNA library in which the cDNAs from PEER(−) cells were subtracted from those from PEER(+) cells. After the SSH subtraction, the cDNAs for the MAPK phosphatases were enriched. One of these clones (named 1–20) contained 600 bases of sequence highly homologous to a leukocyte-specific PTP (LCPTP), also known as hematopoietic tissue-specific PTP (HePTP), a sequence which was originally isolated as a cytoplasmic PTP [19,20].

However, 1–20 contained another 150 bases of unique sequence and thus a phage cDNA library from the activated PEER cells was screened to obtain the full-length cDNA. The translation of the full length 1–20 (DDSP) cDNA sequence revealed one long open reading frame consisting of 293 amino acid (aa) residues, and also a striking homology (96% homology at the aa level) to LCPTP/HePTP (Fig. 1a). In the 50 aa residues of the LCPTP/HePTP N-terminus, there were 3 methionine (Met) residues: translation initiation Met 1 for LCPTP, translation initiation Met 22 for HePTP and Met 49 (Fig. 1b). A putative translation initiation Met for 1–20 corresponded to Met 49 of the LCPTP. And the preceding 24 nt of the 5′ noncoding sequence were identical to those of LCPTP/HePTP (sequence encoding aa residues 41 to 48 of LCPTP, as shown by the thin line above the nucleotide sequence preceding the translation initiation Met for 1–20 in Fig. 1a). However, about 150 bases of the sequence further upstream, including 2 in-frame termination codons, were unique. Although the aa sequence known as the PTP/DSP central catalytic domain was highly conserved, the striking homology to LCPTP/HePTP was disrupted at the C-terminal end, resulting in 11 novel aa sequences (Fig. 1a). Interestingly, the first 25 nt sequences encoding these 11 aa residues were identical to the partial sequence reported for the exon 9/intron 9 junction of LCPTP/HePTP [22].

A BLAST search of the human genome sequence using the 5′- and 3′-noncoding regions of 1–20 assigned each sequence to within the PTPN7 locus on chromosome 1q31 (the 5′-noncoding sequence was the intron 2/exon 3 junction, and the 3′-noncoding sequence was the read-through of the exon 9/intron 9 junction downstream to intron 9) that encodes LCPTP/HePTP, thus strongly suggesting that the 1–20 sequence was a novel alternatively spliced variant of the PTPN7 gene. Another RT-PCR experiment using RNA from human peripheral blood lymphocytes with or without reverse transcription confirmed that the full-length cDNA derived from the mRNA (data not shown).

3.2. Phosphatase activity

To test whether or not clone 1–20 possessed phosphatase activities, a GST fusion product with 1–20 was expressed in SF-9 insect cells since bacterially expressed fusion proteins always formed inclusion bodies. SDS-PAGE showed a stably expressed fusion protein with the expected molecular weight (data not shown). The expressed protein showed a rapid loss of phosphate from the phosphotyrosine in a time dependent manner. The activity was strongest at pH 6.0, and was suppressed by the PTP specific inhibitor sodium orthovanadate (Na_3VO_4) (Fig. 2a). In contrast to LCPTP/HePTP, the expressed 1–20 protein also caused a rapid loss of the phosphate from the phosphothreonine. Although threonine phosphatase activity was weaker (about 50% at the optimal pH 8.0) compared to tyrosine phosphatase activity at the optimal pH, the activity was suppressed by sodium fluoride (NaF), a serine/threonine phosphatase specific inhibitor (Fig. 2b).

3.3. Subcellular localization

The DDSP sequence was in-frame ligated into pEGFP generating pEGFP-DDSP which was transfected into COS-7 cells to observe the subcellular localization of GFP fluorescence. The GFP fluorescence was detected solely in the cytoplasm as in the case of LCPTP/HePTP. Furthermore, the distribution of the GFP-fluorescence was homogeneous, suggesting that this protein was not associated with the membrane structure (Fig. 3a). The treatment of the trans-

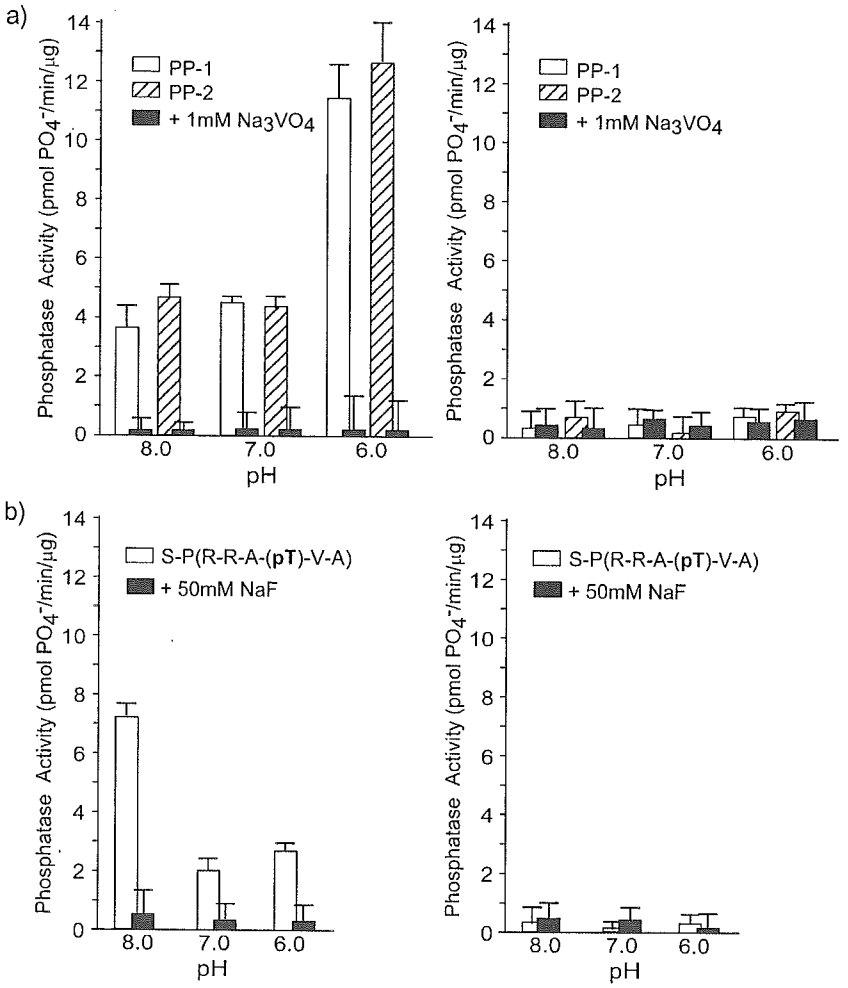

Fig. 2. Phosphatase activities of GST-DDSP. The sequence encoding GST-fused DDSP was ligated into the baculovirus expression vector and expressed in SF-9 cells. (a) Phosphotyrosine phosphatase activity of DDSP (left panel). PP-1 (open column) and PP-2 (dashed column) are 2 different kinds of phosphotyrosine substrate supplied by the manufacturer. Sodium vanadate (Na_3VO_4) is a PTP-specific inhibitor. The phosphatase activity was measured in the absence (open or dashed column) or presence (filled column) of 1 mM Na_3VO_4 and is shown as pmol phosphate released/min/μg of enriched cytosol after passage through a GST-affinity column. The right panel represents the activity of the sample from cells transfected with an empty vector plasmid. (b) Phosphothreonine phosphatase activity of DDSP (left panel). S-P is a phosphothreonine substrate. Sodium fluoride (NaF) is a serine/threonine phosphatase-specific inhibitor. The phosphatase activity was measured in the absence (open) or presence (filled column) of 50 mM NaF. The right panel represents the activity of the sample from cells transfected with an empty vector plasmid.

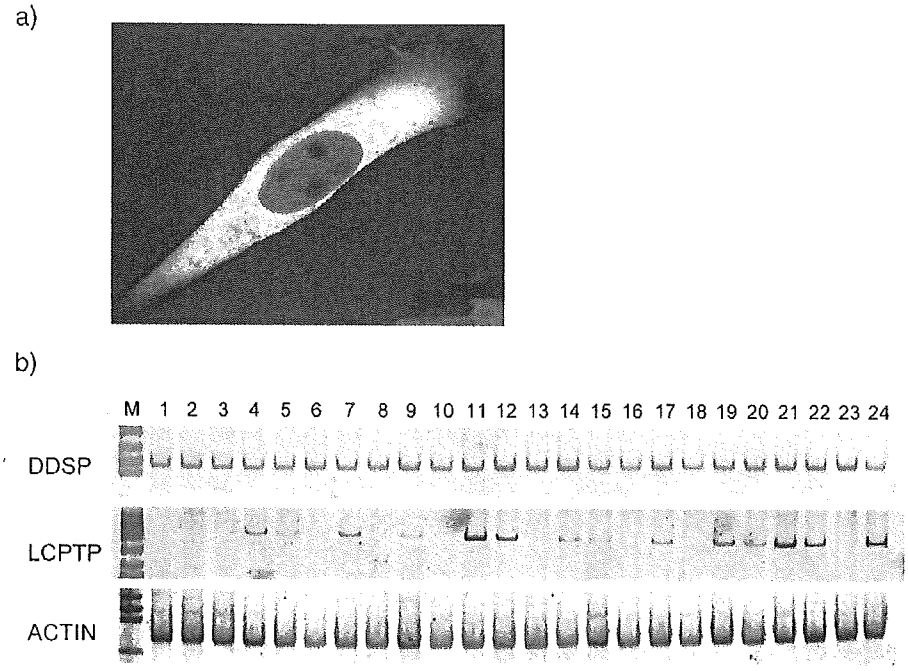

Fig. 3. Subcellular and tissue distribution of DDSP. (a) Cytoplasmic localization of DDSP. The DDSP cDNA sequence was ligated in-frame into pEGFP, transfected into COS7 cells and then subjected to a confocal microscopic analysis. (b) Tissue distribution of DDSP and LCPTP/HePTP. The 2 sequence specific sets of primers for DDSP (top panel) or LCPTP/HePTP (middle panel) were used for RT-PCR. The bottom panel represents the RT-PCR amplifying β-actin mRNA. Lanes are 1: brain; 2: heart; 3: kidney; 4: spleen; 5: liver; 6: colon; 7: lung; 8: small intestine; 9: skeletal muscle; 10: stomach; 11: testis; 12: placenta; 13: salivary gland; 14: thyroid; 15: adrenal; 16: pancreas; 17: ovary; 18: uterus; 19: prostate; 20: skin; 21: lymphocyte; 22: bone marrow; 23: fetal brain; 24: fetal liver.

fected cells with DHEA or treatment of the transfected PEER with or without PMA and A23187 did not significantly change the homogeneous cytoplasmic distribution of GFP-fluorescence (data not shown). Taken together with the observations of the DSP activities, these results indicated that 1–20 encoded a novel member of the cytoplasmic DSP family. We tentatively named this novel DSP DHEA-enhanced DSP (DDSP).

3.4. Profiles of tissue distribution, PMA/A23187 induction and hormonal regulation of DDSP mRNA

To discriminate the mRNA expression of DDSP (full-length 1–20) as potentially DSP from those of tissue-specific LCPTP/HePTP, we designed 2 sets of primers for RT-PCR experiments: one to amplify the sequence specific to DDSP and another specific to LCPTP/HePTP (Fig. 1b). Using these 2 sets of primers, we investigated the tissue distribution and the response to PMA/A23187 or hormonal stimulation. In strong contrast to the restricted tissue distribution of LCPTP/HePTP mRNA preferentially expressed in hematopoietic tissues (and in testis at RT-PCR level), the basal expression of DDSP mRNA was observed by RT-PCR at a similar expression level in all types of human tissues examined (Fig. 3b).

In PEER cells without PMA/A23187 stimulation, the basal expression level (standardized by the fragment length and β-actin expression) of DDSP mRNA was about 20 to 30% of that of LCPTP/HePTP. PMA/A23187 treatment rapidly increased the DDSP mRNA expression within 1 h and then reached a maximum level (5- to 7-fold) at 3 h poststimulation. 100 nM DHEA further increased the DDSP mRNA level by 2.5- to 3-fold at 3 h poststimulation (Fig. 4a). On the other hand, LCPTP/HePTP-specific RT-PCR showed a constitutive expression even in the untreated PEER cells, and PMA/A23187 stimulation with or without DHEA did not significantly alter the expression (Fig. 4b). Costimulation with either 100 nM dexamethasone (DEX), 1 μM DHEA sulfate (DHEAS) or 10 nM dihydrotestosterone (DHT) did not exert the reproducible induction of DDSP mRNA level in the repeated experiments, while the 10 nM 17β-estradiol (E2) treatment sometimes slightly repressed the PMA/A23187-induced DDSP expression. These steroid hormones, including DHEA, did not affect the mRNA levels of LCPTP/HePTP. In Fig. 4c and d, representative results of RT-PCR experiments were shown.

3.5. Interaction of DDSP with the MAPK cascade

To observe the interactions of DDSP with MAPK, we transfected a plasmid expressing a flag-DDSP fusion product into NIH3T3 mouse fibroblasts and then tested the binding of DDSP with activated endogenous ERK1/2, p38-MAPK or JNK by immunocoprecipitation. Western blotting showed that DDSP specifically bound to phosphorylated p38-MAPK activated by hyperosmotic 0.5M NaCl stimulation, but not to

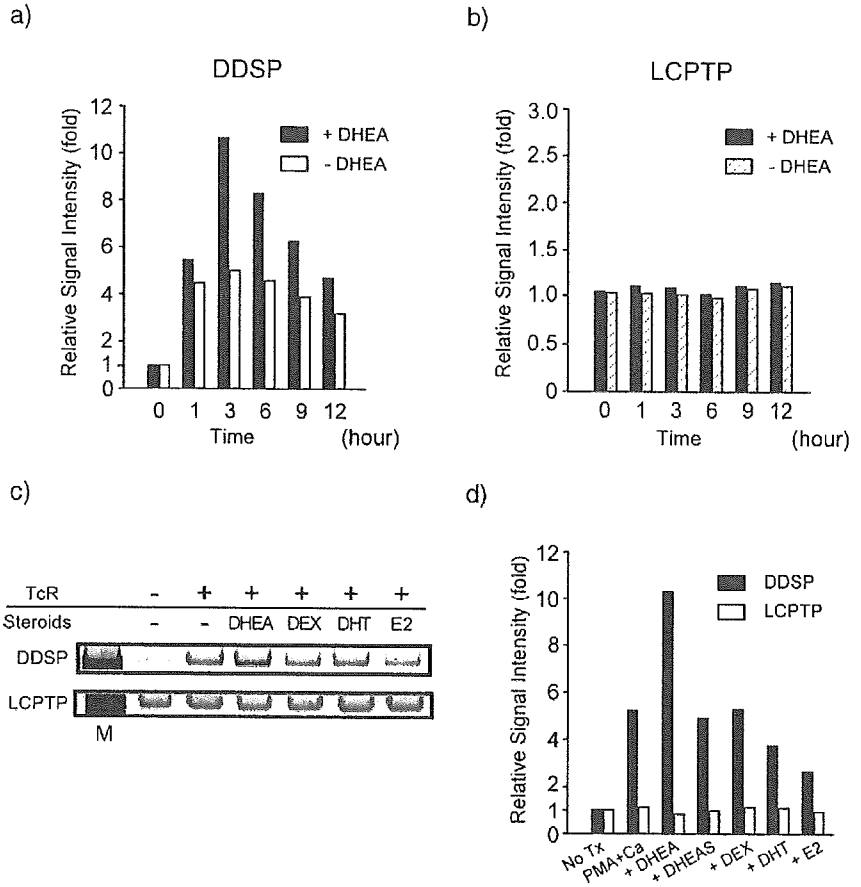

Fig. 4. The differential profiles of mRNA induction between DDSP and LCPTP/HePTP. The same primer set used in Fig. 3b was used for the RT-PCR. (a) The effect of a physiological concentration (100 nM) of DHEA on the expression of DDSP in TcR-activated PEER cells. PEER cells were stimulated by PMA and calcium ionophore A23187 with (filled bar) or without (open bar) DHEA. The relative induction values compared with the basal mRNA expression with no PMA/A23187 treatment, standardized by β-actin expression, are expressed as the-fold induction. (b) Effect of 100 nM DHEA on the expression of LCPTP/HePTP in TcR-activated PEER cells. PEER cells were stimulated as described above. The relative induction values are expressed as in Panel (a). Filled bars: with DHEA; hatched bars: without DHEA. (c) Effects of various steroid hormones on the mRNA expression of DDSP or LCPTP/HePTP. Representative results of the RT-PCR experiments are shown. The PEER cells were treated with PMA and calcium ionophore A23187 in the absence of any steroid hormones, or in the presence of 100 nM DHEA (DHEA), 100 nM dexamethasone (DEX), 10 nM dihydrotestosterone (DHT), or 1 nM 17β-estradiol (E2). The RNAs were extracted after 3 h of treatment and then subjected to semiquantitative RT-PCR using a set of primers specific for DDSP (upper panel) or LCPTP/HePTP (lower panel). (d) Schematic representation of the effects of the various steroid hormones. In this experiment, treatment with 1 μM of DHEA-sulfate (DHEAS) was included. The relative induction of each sequence in the PEER cells compared with the basal mRNA expression with no treatment (No Tx) is expressed as the-fold induction. The PEER cells were treated with PMA and calcium ionophore A23187 in the absence of any steroid hormones (PMA+Ca) or in the presence of 100 nM DHEA (DHEA), 1 μM DHEAS (DHEAS), 100 nM dexamethasone (DEX), 10 nM dihydrotestosterone (DHT) or 1 nM 17β-estradiol (E2), respectively. Filled bars: DDSP mRNA; open bars: LCPTP/HePTP mRNA.

activated ERK1/2 or JNK (Fig. 5a and b). This finding also suggested that the N-terminal 13 aa residues of DDSP (corresponding to aa residues 49–61 of LCPTP) were required for and enough for P38-MAPK-binding.

The inactivation of the phosphorylated p38-MAPK by DDSP was shown by the dephosphorylation of the phosphorylated p38-MAPK. DDSP specifically dephosphorylated the endogenous p38-MAPK, activated by hyperosmotic stimulation using 0.5 M NaCl, in NIH3T3 cells that were transiently transfected with plasmids expressing flag-tagged DDSP, while the phosphorylated ERK or JNK were not dephosphorylated (Fig. 6a). The p38-MAPK-specific inactivation was further confirmed using the pMACS system that can select transfected cells from untransfected cells and can thus enrich the transfected cells to nearly 80% after passage through an affinity column. The expression of the DDSP protein dephosphorylated the endogenous p38-MAPK activated by 0.4 M sorbitol hyperosmotic treatment, but not ERK activated by PMA treatment, in the cells selected after the enrichment (Fig. 6b). Taken together, these results indicated that DDSP inactivates the MAPK cascade in a p38-MAPK-specific fashion.

4. Discussion

To clarify the action of DHEA on a molecular basis, a comparison of the cellular phenotypes between the DHEA-

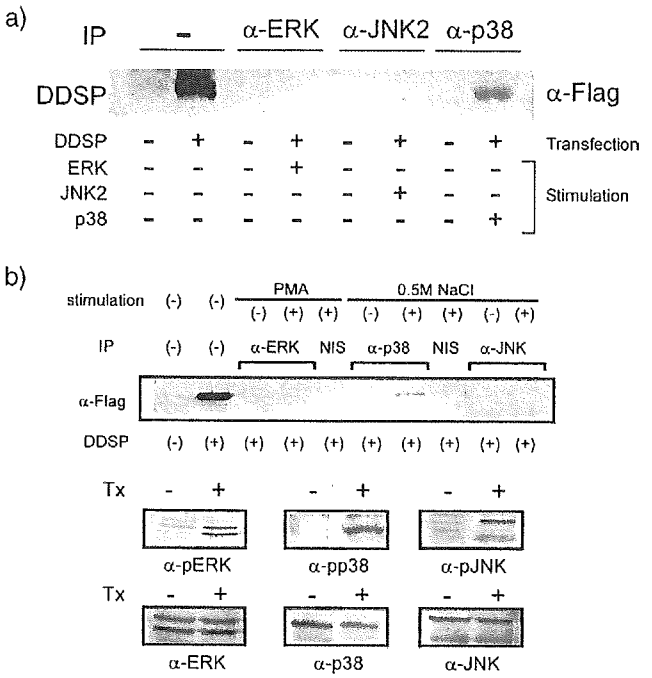

Fig. 5. Immunocoprecipitation of DDSP with ERK, p38 or JNK. (a) NIH3T3 cells transfected with a plasmid expressing flag-tagged DDSP were treated with 0.5 M NaCl for 20 min (for p38 and JNK) or with 50 ng/ml of PMA for 15 min after incubation in a serum free medium for 15 h (for ERK). The endogenous ERK, p-38 or JNK in the whole cell lysates from the treated cells was immunoprecipitated with an anti-ERK, -p38 or -JNK antibody, respectively, and then Western blotting was performed using an anti-flag antibody. DDSP specifically interacts with the endogenous phosphorylated p38-MAPK. (b) Immunoprecipitation and Western blot were performed as in Panel (a) (top panel). NIS: non-immune serum. In the middle and bottom panels, the three pairs of whole cell lysates used for the immunoprecipitations in the top panel were probed to confirm the activation of each MAPK, using antibodies against phosphorylated MAPKs (middle panels: anti-pERK, anti-pp38, anti-pJNK) or total MAPKs (bottom panels: anti-ERK, anti-p38, anti-JNK). Tx: PMA-treatment for the activation of ERK or 0.5 M NaCl treatment for the activation of p38- or JNK-MAPK.

treated and untreated cells led to the isolation of the p38 MAPK phosphatase, DDSP. We demonstrated that this novel member of the PTPN7 locus-derived family was a candidate for one of the target genes of DHEA. One explanation for the biological action of DHEA is that DHEA exerts its functions after being biotransformed into biologically more active androgens and estrogens in either the peripheral tissues or the target cells (intracrine mechanism) [23]. In contrast, the superinduction effect of DHEA on the DDSP mRNA level was specific according to the results shown in Fig. 4. As one of the broad range of actions caused by DHEA, DHEA(-S) has been used for some collagen disease as adjunctive treatment expecting the immune modulating action [24–27] (for review). In this regard, the lymphocytes from the periphery of systemic lupus erythematosus (SLE) patients had a more activated p38 MAPK, as well as ERK or JNK, status immediately ex vivo when compared with lymphocytes from the periphery of normal individuals [28].

We propose a mechanism to explain, at least in part, this immune modulating action, namely that DHEA exerts the anti-inflammatory action by directly suppressing the p38-MAPK cascade. Recently, p38-MAPK has received much attention as a potential drug target for diseases such as rheumatoid arthritis, endotoxic shock, inflammatory bowel disease, osteoporosis and many others [29]. Our findings suggest that DHEA augments the negative feedback regulation of MAPK cascades that have become overactivated due to stress or cytokine signals via a specific set of MAPK phosphatases in many human tissues. In the vascular smooth muscle cell, p38-MAPK activation by PDGF is inhibited by low molecular weight PTPs, thus suggesting that MAPK phosphatases are important negative regulators for the vascular smooth muscle cell growth and migration processes leading to the progression of atherosclerosis [8,9,30]. Apart from the action on the MAPK cascade, it has been demonstrated that DHEA inhibits the nuclear translocation of nuclear factor-κB (NF-κB) probably due to the induction of peroxisome via the peroxisome proliferator activated receptor α (PPARα) [31], or that DHEA inhibits the binding of transcription factor activator protein-1 (AP-1) to DNA [32], thus exerting the anti-inflammatory action. To date, no receptor for DHEA or DHEAS has yet been cloned. The presence of cytoplasmic DHEA binding activity has been demonstrated in human peripheral blood monocytes [7], vascular smooth muscle cell [9] and human T lymphocytes [16], although according to the human genome project, it seems unlikely that a classical steroid hormone receptor-type DHEA receptor exists. Interestingly, Liu et al. reported the existence of the putative membrane receptor for DHEA [33]. DHEA may directly exert its

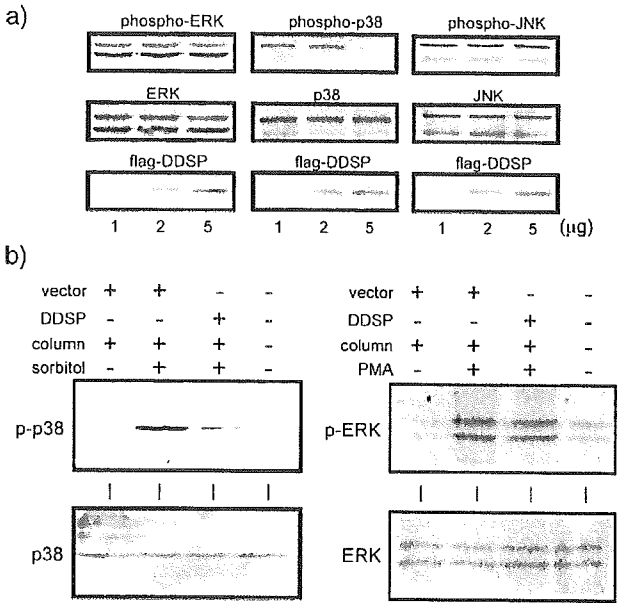

Fig. 6. DDSP dephosphorylates p38-MAPK. (a) Phosphatase activities of DDSP on ERK, p38 or JNK. NIH3T3 cells were transfected with 1, 2 or 5 μg of a plasmid expressing flag-tagged DDSP (left lane, middle lane and right lane, respectively, in each panel). The total amounts of the transfected plasmids were kept constant by adding the empty vector plasmid. The transfected cells were treated as in Fig. 5, and then the whole cell lysates were subjected to Western blotting. The antibodies were raised against phosphorylated (phospho-) MAPKs (top panels), total MAPKs (middle panels) or flag (bottom panels). (b) pMACS experiment showing the p38-MAPK-specific dephosphorylation. NIH3T3 cells were transfected in 10 cm dishes with 20 μg of pMACS-DDSP (DDSP), or pMACSKkII vector (vector) as a control. The transfected cells were enriched after column separation and then treated with 0.4 M sorbitol for 20 min to activate p38-MAPK or with 50 ng/ml PMA to activate ERK. Western blotting was performed using an antibody against phosphorylated p38-MAPK (upper left) or ERK (upper right) (shown as p-p38 and p-ERK, respectively) or total p38-MAPK (lower left) or ERK (lower right) (shown as p38 and ERK, respectively). In this experiment, the column passage alone mildly activated p38-MAPK and caused the basal level phosphorylation of p38-MAPK. The expression of DDSP specifically inactivated the p38-MAPK to the basal level.

action not through the nuclear receptor but through the signal transduction system, such as MAPK system, activated by membrane-type receptors.

The MAPK cascade is regulated by both the phosphorylation and dephosphorylation of the members of the cascade. LCPTP/HePTP has been shown to act as a phosphotyrosine-specific phosphatase for both ERK (ERK2) and p38-MAPK [34,35], and one report showed HePTP as the ERK2-specific phosphatase in the myelogenous leukemia cell line K562 [36]. While LCPTP/HePTP does not dephosphorylate phosphoserine/phosphothreonine residues in ERK1/2 [34], recent findings have revealed that a subfamily of PTP dephosphorylate not only the phosphotyrosine but also the phosphoserine/phosphothreonine residue, and was thus called DSP [37]. When we tested whether or not the DDSP protein possesses phosphatase activities for the phosphoserine/phosphothreonine residue, the DDSP protein also caused a rapid loss of the phosphate from the phosphothreonine as well as from the phosphotyrosine. These results indicated that the DDSP might play a role as a DSP in vivo.

Each DSP or PTP has a restricted subcellular localization [37] (for review), while LCPTP/HePTP has been shown to localize in the cytoplasm (cytoplasmic PTP) as well [38]. DDSP was cytoplasmic as well as LCPTP/HePTP. In contrast, the mRNA profiles of the tissue distribution and the response to MAPK cascade stimulation and steroid hormone treatment were different between DDSP and LCPTP/HePTP, while DDSP was highly homologous to LCPTP/HePTP. Although the mRNA expression of LCPTP/HePTP has previously been shown to be inducible, the RT-PCR experiments using specific sets of primers suggested that the expression of LCPTP/HePTP was constitutive while the actual inducible sequence could be that of DDSP. While mRNA levels in mouse lymphocytes, detected by Northern blots, increased upon stimulation with phytohemagglutinin, lipopolysaccharide, concanavalin A, or anti-CD3 [20], the HePTP protein was present even in resting cells, and its amount increased slightly [34]. The differential mRNA expression between DDSP and LCPTP/HePTP might be due to, though not to be tested yet, the differential promoter usage.

In addition, at the protein level, the substrate specificity was different between DDSP and LCPTP/HePTP. LCPTP/HePTP binds to both ERKs and p38-MAPK through a kinase-interaction motif (KIM) located at the N-terminus of the protein and inactivates them by dephosphorylating the critical phosphotyrosine residue in their activation loop, thus playing a negative role in the TcR signaling pathway [39]. Furthermore, the binding of HePTP to ERK or p38-MAPK is in a phosphorylation-independent fashion [34]. HePTP has previously been shown to interact with both ERK1/2 and p38-MAPK via the 40 aa of the N-terminus sequence [34]. The aa residues 1 to 40 of HePTP corresponded to aa residues 22 to 61 of LCPTP (Fig. 1b). In particular, Arg41 and Arg42 play a crucial role in ERK binding [35]. DDSP lacked the first 48 aa stretch (including Arg41 and Arg42) of LCPTP required for ERK1/2 binding, while the following aa sequence was highly conserved, except for 1 aa residue (Val 220, bold line in Fig. 1b) in addition to the unique 11 aa stretch at the C′ -terminus end (Fig. 1a). This may contribute to why DDSP specifically bound to and inactivated phosphorylated p38-MAPK. To date, only one molecule, Wip1, which is induced in response to ionizing radiation in a p53-dependent manner, has been shown to be a p38-specific MAPK phosphatase [40,41]. Our present study suggested the complexity of the gene regulation in the PTPN7 locus. By the mechanisms of alternative splicing and possible differential promoter usage, PTPN7 may encode at least 3 protein phosphatases: one is the inducible DDSP specifically inactivating p38-MAPK and the others are constitutively expressed PTPs inactivating both ERK and p38-MAPK.

Acknowledgements

We would like to thank Otsuka Pharmaceutical Co. Ltd., Japan, for valuable discussions and help during the SSH screening.

References

[1] R.J. Davis, The mitogen-activated protein kinase signal transduction pathway, J. Biol. Chem. 268 (1993) 14553–14556.
[2] Z. Galcheva-Gargova, B. Derijard, I.H. Wu, R.J. Davis, An osmosensing signal transduction pathway in mammalian cells, Science 265 (1994) 806–808.
[3] J.M. Kyriakis, P. Banerjee, E. Nikolakaki, T. Dai, E.A. Rubie, M.F. Ahmad, J. Avruch, J.R. Woodgett, The stress-activated protein kinase subfamily of c-*Jun* kinases, Nature 369 (1994) 156–160.
[4] E. Cano, L.C. Mahadevan, Parallel signal processing among mammalian MAPKs, Trends Biochem. Sci. 20 (1995) 117–122.
[5] R. Seger, E.G. Krebs, The MAPK signaling cascade, FASEB J. 9 (1995) 726–735.
[6] S. Tamura, M. Hanada, M. Ohnishi, K. Katsura, M. Sasaki, T. Kobayashi, Regulation of stress-activated protein kinase signaling pathways by protein phosphatases, Eur. J. Biochem. 269 (2002) 1060–1066.
[7] J.A. McLachlan, C.D. Serkin, O. Bakouche, Dehydroepiandrosterone modulation of lipopolysaccharide-stimulated monocyte cytotoxicity, J. Immunol. 156 (1996) 328–335.
[8] T. Yoshimata, A. Yoneyama, Y. Jin-no, N. Tamai, Y. Kamiya, Effects of dehydroepiandrosterone on mitogen-activated protein kinase in human aortic smooth muscle cells, Life Sci. 65 (1999) 431–440.
[9] M.R. Williams, S. Ling, T. Dawood, K. Hashimura, A. Dai, H. Li, J.P. Liu, J.W. Funder, K. Sudhir, P.A. Komesaroff, Dehydroepiandrosterone inhibits human vascular smooth muscle cell proliferation independent of ARs and ERs, J. Clin. Endocrinol. Metab. 87 (2002) 176–181.
[10] A.J. Morales, J.J. Nolan, J.C. Nelson, S.S. Yen, Effects of replacement dose of dehydroepiandrosterone in men and women of advancing age, J. Clin. Endocrinol. Metab. 78 (1994) 1360–1367.
[11] F. Labrie, P. Diamond, L. Cusan, J.L. Gomez, A. Belanger, B. Candas, Effect of 12-month dehydroepiandrosterone replacement therapy on bone, vagina, and endometrium in postmenopausal women, J. Clin. Endocrinol. Metab. 82 (1997) 3498–3505.
[12] W. Arlt, F. Callies, J.C. van Vlijmen, I. Koehler, M. Reincke, M. Bidlingmaier, D. Huebler, M. Oettel, M. Ernst, H.M. Schulte, B. Allolio, Dehydroepiandrosterone replacement in women with adrenal insufficiency, N. Engl. J. Med. 341 (1999) 1013–1020.
[13] E.E. Baulieu, G. Thomas, S. Legrain, N. Lahlou, M. Roger, B. Debuire, V. Faucounau, L. Girard, M.P. Hervy, F. Latour, M.C. Leaud, A. Mokrane, H. Pitti-Ferrandi, C. Trivalle, O. de Lacharriere, S. Nouveau, B. Rakoto-Arison, J.C. Souberbielle, J. Raison, Y. Le Bouc, A. Raynaud, X. Girerd, F. Forette, Dehydroepiandrosterone (DHEA), DHEA sulfate, and aging: contribution of the DHEAge Study to a sociobiomedical issue, Proc. Natl. Acad. Sci. U. S. A. 97 (2000) 4279–4284.
[14] H. Nawata, T. Yanase, K. Goto, T. Okabe, K. Ashida, Mechanism of action of anti-aging DHEA-S and the replacement of DHEA-S, Mech. Ageing Dev. 123 (2002) 1101–1106.
[15] Z. Ravid, N. Goldblum, R. Zaizov, M. Schlesinger, T. Kertes, J. Minowada, W. Verbi, M. Greaves, Establishment and characterization of a new leukaemic T-cell line (Peer) with an unusual phenotype, Int. J. Cancer 25 (1980) 705–710.
[16] T. Okabe, M. Haji, R. Takayanagi, M. Adachi, K. Imasaki, F. Kurimoto, T. Watanabe, H. Nawata, Up-regulation of high-affinity dehydroepiandrosterone binding activity by dehydroepiandrosterone in activated human T lymphocytes, J. Clin. Endocrinol. Metab. 80 (1995) 2993–2996.
[17] J.N. Siegel, R.D. Klausner, U.R. Rapp, L.E. Samelson, T cell antigen receptor engagement stimulates c-raf phosphorylation and induces c-raf-associated kinase activity via a protein kinase C-dependent pathway, J. Biol. Chem. 265 (1990) 18472–18480.
[18] M. Izquierdo, S. Bowden, D. Cantrell, The role of Raf-1 in the regulation of extracellular signal-regulated kinase 2 by the T cell antigen receptor, J. Exp. Med. 180 (1994) 401–406.
[19] M. Adachi, M. Sekiya, M. Isobe, Y. Kumura, Z. Ogita, Y. Hinoda, K. Imai, A. Yachi, Molecular cloning and chromosomal mapping of a human protein–tyrosine phosphatase LC-PTP, Biochem. Biophys. Res. Commun. 186 (1992) 1607–1615.
[20] B. Zanke, H. Suzuki, K. Kishihara, L. Mizzen, M. Minden, A. Pawson, T.W. Mak, Cloning and expression of an inducible lymphoid-specific, protein tyrosine phosphatase (HePTPase), Eur. J. Immunol. 22 (1992) 235–239.
[21] M. Saxena, S. Williams, K. Tasken, T. Mustelin, Crosstalk between cAMP-dependent kinase and MAP kinase through a protein tyrosine phosphatase, Nat. Cell Biol. 1 (1999) 305–311.
[22] M. Adachi, T. Miyachi, M. Sekiya, Y. Hinoda, A. Yachi, K. Imai, Structure of the human LC-PTP (HePTP) gene: similarity in genomic organization within protein-tyrosine phosphatase genes, Oncogene 9 (1994) 3031–3035.
[23] F. Labrie, A. Belanger, J. Simard, L.-T. Van, C. Labrie, DHEA and peripheral androgen and estrogen formation: intracinology, Ann. N.Y. Acad. Sci. 774 (1995) 16–28.
[24] R.H. Derksen, Dehydroepiandrosterone (DHEA) and systemic lupus erythematosus, Semin. Arthritis Rheum. 27 (1998) 335–347.
[25] D.M. Chang, J.L. Lan, H.Y. Lin, S.F. Luo, Dehydroepiandrosterone treatment of women with mild-to-moderate systemic lupus erythematosus: a multicenter randomized, double-blind, placebo-controlled trial, Arthritis Rheum. 46 (2002) 2924–2927.
[26] M.A. Petri, R.G. Lahita, R.F. Van Vollenhoven, J.T. Merrill, M. Schiff, E.M. Ginzler, V. Strand, A. Kunz, K.J. Gorelick, K.E. Schwartz, Effects of prasterone on corticosteroid requirements of women with systemic lupus erythematosus: a double-blind, randomized, placebo-controlled trial, Arthritis Rheum. 46 (2002) 1820–1829.
[27] R.F. van Vollenhoven, Dehydroepiandrosterone in systemic lupus erythematosus, Rheum. Dis. Clin. North Am. 26 (2000) 349–362.
[28] A.C. Grammer, R. Fischer, O. Lee, X. Zhang, P.E. Lipsky, Flow cytometric assessment of the signaling status of human B lymphocytes from normal and autoimmune individuals, Arthritis Res. Ther. 6 (2004) 28–38 (Electronic publication 2004 Feb 2005).
[29] R.L. Thurmond, S.A. Wadsworth, P.H. Schafer, R.A. Zivin, J.J. Siekierka, Kinetics of small molecule inhibitor binding to p38 kinase, Eur. J. Biochem. 268 (2001) 5747–5754.
[30] H. Shimizu, M. Shiota, N. Yamada, K. Miyazaki, N. Ishida, S. Kim, H. Miyazaki, Low M(r) protein tyrosine phosphatase inhibits growth and migration of vascular smooth muscle cells induced by platelet-derived growth factor, Biochem. Biophys. Res. Commun. 289 (2001) 602–607.
[31] M.E. Poynter, R.A. Daynes, Peroxisome proliferator-activated receptor alpha activation modulates cellular redox status, represses nuclear factor-kappaB signaling, and reduces inflammatory cytokine production in aging, J. Biol. Chem. 273 (1998) 32833–32841.
[32] R. Dashtaki, A.R. Whorton, T.M. Murphy, P. Chitano, W. Reed, T.P. Kennedy, Dehydroepiandrosterone and analogs inhibit DNA binding of AP-1 and airway smooth muscle proliferation, J. Pharmacol. Exp. Ther. 285 (1998) 876–883.
[33] D. Liu, J.S. Dillon, Dehydroepiandrosterone activates endothelial cell nitric-oxide synthase by a specific plasma membrane receptor coupled to Galpha(i2,3), J. Biol. Chem. 277 (2002) 21379–21388 (Electronic publication 22002 Apr 21304).
[34] M. Saxena, S. Williams, J. Brockdorff, J. Gilman, T. Mustelin, Inhibition of T cell signaling by mitogen-activated protein kinase-

targeted hematopoietic tyrosine phosphatase (HePTP), J. Biol. Chem. 274 (1999) 11693–11700.
[35] M. Oh-hora, M. Ogata, Y. Mori, M. Adachi, K. Imai, A. Kosugi, T. Hamaoka, Direct suppression of TCR-mediated activation of extracellular signal-regulated kinase by leukocyte protein tyrosine phosphatase, a tyrosine-specific phosphatase, J. Immunol. 163 (1999) 1282–1288.
[36] S.M. Pettiford, R. Herbst, The MAP-kinase ERK2 is a specific substrate of the protein tyrosine phosphatase HePTP, Oncogene 19 (2000) 858–869.
[37] M. Camps, A. Nichols, S. Arkinstall, Dual specificity phosphatases: a gene family for control of MAP kinase function, FASEB J. 14 (2000) 6–16.
[38] A. Gjorloff-Wingren, M. Saxena, S. Han, X. Wang, A. Alonso, M. Renedo, P. Oh, S. Williams, J. Schnitzer, T. Mustelin, Subcellular localization of intracellular protein tyrosine phosphatases in T cells, Eur. J. Immunol. 30 (2000) 2412–2421.
[39] M. Saxena, S. Williams, J. Gilman, T. Mustelin, Negative regulation of T cell antigen receptor signal transduction by hematopoietic tyrosine phosphatase (HePTP), J. Biol. Chem. 273 (1998) 15340–15344.
[40] M. Fiscella, H. Zhang, S. Fan, K. Sakaguchi, S. Shen, W.E. Mercer, G.F. Vande Woude, P.M. O'Connor, E. Appella, Wip1, a novel human protein phosphatase that is induced in response to ionizing radiation in a p53-dependent manner, Proc. Natl. Acad. Sci. U. S. A. 94 (1997) 6048–6053.
[41] M. Takekawa, M. Adachi, A. Nakahata, I. Nakayama, F. Itoh, H. Tsukuda, Y. Taya, K. Imai, p53-inducible wip1 phosphatase mediates a negative feedback regulation of p38 MAPK-p53 signaling in response to UV radiation, EMBO J. 19 (2000) 6517–6526.

0013-7227/05/$15.00/0
Printed in U.S.A.

Endocrinology 146(1):85–92

doi: 10.1210/en.2004-1046

Activation of Peroxisome Proliferator-Activated Receptor-γ and Retinoid X Receptor Inhibits Aromatase Transcription via Nuclear Factor-κB

WuQiang Fan, Toshihiko Yanase, Hidetaka Morinaga, Yi-Ming Mu, Masatoshi Nomura, Taijiro Okabe, Kiminobu Goto, Nobuhiro Harada, and Hajime Nawata

Department of Medicine and Bioregulatory Science (W.F., T.Y., H.M., M.N., T.O., K.G., H.N.), Graduate School of Medical Science, Kyushu University, Fukuoka 812-8582 Japan; Core Research for Evolutional Science and Technology (CREST) (T.Y., H.M., M.N., T.O., K.G., H.N.), Japan Science and Technology Corporation, Kawaguchi, Saitama 332-0012, Japan; Department of Endocrinology (Y.-M.M.), Chinese PLA General Hospital, Beijing 100853, China; and Department of Biochemistry (N.H.), School of Medicine, Fujita Health University, 470-1192 Aichi, Japan

Our previous studies demonstrated that a peroxisome proliferator-activated receptor (PPAR)-γ ligand, troglitazone (TGZ), and/or a retinoid X receptor (RXR) ligand, LG100268 (LG), decreased the aromatase activity in both cultured human ovarian granulosa cells and human granulosa-like tumor KGN cells. In the present study, we further found that a combined treatment of TGZ+LG decreased aromatase promoter II (ArPII) activity in both ovarian KGN cells and fibroblast NIH-3T3 cells in a PPARγ-dependent manner. Furthermore, the inhibition of both aromatase activity and the transcription of ArPII by TGZ+LG was completely eliminated when nuclear factor-κB (NF-κB) signaling was blocked by specific inhibitors, suggesting NF-κB, which is endogenously expressed in both fibroblast and granulosa cells, might be a mediator of this inhibition. Interestingly, activation of NF-κB by either forced expression of the p65 subunit or NF-κB-inducing kinase up-regulated ArPII activity. Positive regulation of aromatase by endogenous NF-κB was also suggested by the fact that NF-κB-specific inhibitors suppress basal activity of the aromatase gene. A concomitant formation of high-order complex between NF-κB p65 and ArPII was also observed by chromatin immunoprecipitation assay. Although activation of PPARγ and RXR affected endogenous expression levels of neither inhibitory κBα nor p65, it impaired the interaction between NF-κB and ArPII and the p65 based transcription as well. Altogether, these results indicate that activation of a nuclear receptor system, constituted by PPARγ and RXR, down-regulates aromatase expression through the suppression of NF-κB-dependent aromatase activation and thus provide a new insight in the mechanism of regulation of the aromatase gene. (*Endocrinology* 146: 85–92, 2005)

THE BIOSYNTHESIS OF estrogens is catalyzed by the enzyme complex referred to as aromatase cytochrome P-450, which aromatizes the A ring of C19 androgens to the phenolic A ring of C18 estrogens, resulting in loss of the C19 angular methyl group as formic acid (1). In humans, aromatase is present in many tissues, including ovary (2, 3), testis (4, 5), placenta (2), and brain (6, 7). The gene encoding the aromatase (*CYP19*) is extraordinarily long (more than 120 kb), with a coding region of approximately 30 kb, containing nine translated exons (II-X). One reason for this long gene is that the transcription of aromatase in different tissue is regulated by different promoters (8) (ovary: promoter II; placenta: promoter I.1; and adipose tissue: promoter I.4). The aromatase promoter II (ArPII) functions in the ovary under the control of FSH. In cooperation with Ad4BP/SF-1, FSH, via the cAMP-protein kinase A (PKA) pathway, stimulates aromatase gene expression in the ovary through promoter II.

It has been determined that estrogens contribute to the growth and development of some estrogen-dependent neoplasm, including breast, endometrial cancers, and some ovarian cancers (9, 10). Estrogens, especially those produced locally in the adipose stoma cells, exert a definite role in stimulating proliferation of breast tumor cells (11). In normal breast adipose tissue, the estrogen-producing aromatase gene is driven by a distal promoter I.4 (8), whereas in breast adipose tissue containing a tumor, there is a switch in the promoter, whereby the aromatase expression is regulated through the proximal promoter II. This shift results in elevated aromatase expression in the tumor or surrounding breast adipose tissue and subsequently elevated production of estrogen in local breast adipose tissue, thus leading to the development of breast cancer (12–16). These findings highlight the importance of promoter II, especially in breast cancer.

Peroxisome proliferator-activated receptor (PPAR)-γ is a nuclear receptor that has an essential role in adipogenesis and glucose homeostasis in response to its ligands, which are either naturally existing ligands like 15-deoxy-$\Delta^{12,14}$ prostaglandin J2 or synthetic thiazolidinediones. Besides relatively

First Published Online September 30, 2004

Abbreviations: APDC, Ammonium pyrrolidinedithiocarbamate; ArPII, aromatase promoter II; CAPE, caffeic acid phenethyl ester; ChIP, chromatin immunoprecipitation; CMV, cytomegalovirus; DMSO, dimethyl sulfoxide; FBS, fetal bovine serum; IκBα, inhibitory κBα; LG, LG100268; NF-κB, nuclear factor-κB; NIK, NF-κB-inducing kinase; NS, normal saline; PKA, protein kinase A; PPAR, peroxisome proliferator-activated receptor; RXR, retinoid X receptor; SDS, sodium dodecyl sulfate; TGZ, troglitazone.

Endocrinology **is published monthly by The Endocrine Society (http://www.endo-society.org), the foremost professional society serving the endocrine community.**

well-known PPARγ-expressing tissues like adipose tissue, adrenal gland, and spleen (17–19), ovary (20) and granulosa cells (21, 22) also express an abundant amount of PPARγ, whose physiological role in these tissues is largely unknown. We previously reported that the PPARγ ligand, troglitazone (TGZ), especially together with the retinoid X receptor (RXR) ligand, LG100268 (LG), dose-dependently inhibits aromatase activity in granulosa cells (21, 23, 24).

In the present study, we extended our study to clarify the underlying mechanism whereby activation of a nuclear receptor system constituted by PPARγ and RXR down-regulates the aromatase gene. Herein we report an involvement of the transcriptional factor nuclear factor-κB (NF-κB) in the above mechanism as well as its importance in the regulation of aromatase expression through promoter II.

Materials and Methods

Materials

TGZ and LG were obtained from Sankyo Pharmaceuticals (Tokyo, Japan), and Ligand Pharmaceuticals Inc. (San Diego, CA), respectively. Caffeic acid phenethyl ester (CAPE), forskolin, and TNFα were all purchased from Sigma-Aldrich (St. Louis, MO). Ammonium pyrrolidinedithiocarbamate (APDC) was purchased from Wako (Osaka, Japan). All the above compounds (except CAPE and TNFα, which were dissolved in 50% ethanol and normal saline, respectively) were dissolved in dimethyl sulfoxide (DMSO), and the final concentration of solvents (DMSO, 50% ethanol or normal saline) in the cell growth medium was 0.1% (vol/vol). An equal volume of solvents was added to control cultures during cell treatment with chemicals.

Cell culture

We established a human ovarian granulosa-like tumor cell line, KGN, from a 63-yr-old female patient with invasive granulosa cell carcinoma (25). The cells grew as an adherent monolayer with stable proliferation. The cells possess properties similar to those of normal granulosa cells, including the expression of functional FSH receptor and a relatively high aromatase activity, which is PKA dependent (25). The cells were maintained in DMEM/F12 supplemented with 10% fetal bovine serum (FBS) in an atmosphere of 5% CO_2 at 37 C. NIH-3T3 cells were purchased from the Japanese Cell Research Bank (Tokyo) and maintained in DMEM (high glucose) supplemented with 10% FBS at 37 C.

Aromatase assay

The aromatase activity was determined by measuring the $[^3H]H_2O$ released on conversion of [1β-^{3}H]androstenedione to estrone, as described previously (21). The cells were precultured in 6-well plates in DMEM/F12 with 5% dextran-coated, charcoal-treated FBS for 48 h before treatment with chemicals. After the cells were treated with TGZ+LG, [1β-^{3}H]androstenedione was added, and the cells were then further incubated for 6 h. In the case of combined treatment with the NF-κB inhibitors, CAPE or APDC was added to cultures 2 h before an 8-h treatment with TGZ+LG. A second-round treatment consisting of 2 h of CAPE (or ADPC) followed by 8 h of TGZ+LG was carried out before addition of [1β-^{3}H]androstenedione. Extraction of medium (2.0 ml) and measurement of radioactivity in $[^3H]H_2O$ for aromatase activity were done as described previously (21). The amount of radioactivity was then standardized by protein concentration, which was determined using a micro-BCA kit (Pierce Chemical Co., Rockford, IL) and expressed as picomoles per milligram protein per 6 h.

Plasmid constructions

The 4.0-kb ArPII was amplified by PCR from genomic DNA. After confirmation of the entire sequence by direct sequencing, the fragment was subcloned into PGL3-Basic vector (Promega, Madison, WI) to make the luciferase reporter plasmid PGL3-ArPII, in which the luc+ gene is driven by the 4.0-kb fragment of human ArPII. To construct the NF-κB luciferase reporter plasmid, pGL3-tk was first constructed by cloning the −109 to +37 region of the herpes virus thymidine kinase promoter into the *Bgl*II and *Hin*dIII sites of the pGL3-basic vector (Promega). A pair of oligonucleotides, 5′-TGGAAATTCCTGGAAATTCCTGGAAATTCC-3′ and 5′-TCGAGGAATTTCCAGGAATTTCCAGGAATTTCCA-3′, were annealed together, thus resulting in double-stranded oligonucleotides with both a blunt end and a *Xho*I compatible overhang, which were then ligated into the *Sma*I and *Xho*I sites of tk-Luc, thus giving rise to pGL3-NF-κB containing three copies of the NF-κB sites. The *Renilla* luciferase reporter plasmid phRL-cytomegalovirus (CMV), serving as an internal control in the dual-luciferase reporter assay, was purchased from Promega. Human p65 expression vector, pcDNA-p65, was provided by Dr. C. Scheidereit (Max Delbruck Center for Molecular Medicine, Berlin, Germany). pcDNA-NF-κB-inducing kinase (NIK) was provided by Dr. D. Wallach (Department of Biological Chemistry, The Weizmann Institute of Science, Rehovot, Israel). All plasmids were prepared from an overnight bacterial culture using the QIAfilter plasmid maxikit (Qiagen, Valencia, CA).

Relative luciferase reporter assay

For the relative luciferase reporter assay, 1.5×10^5 cells/well in 1 ml growth medium were seeded into 12-well plates, and 0.8 μg of PGL3-ArPII (or PGL3-NF-κB) and 2.0 ng of phRL-CMV were transiently cotransfected in each well using the Superfect transfection reagent (Qiagen) following the manufacturer's protocol. In the case of cotransfection, 0.15 μg of expression vector for p65 (pcDNA-p65) or NIK (pcDNA-NIK) was also added; the total amount of plasmid DNA added to each well was equalized using the empty vector: pcDNA-3.1. Twenty-four hours after transfection, the cells were treated with TGZ+LG for 24 h at the concentrations indicated in each figure. The cells were then lysed in 100 μl/well passive lysis buffer, and the luciferase assay was performed in accordance with the protocol of the dual-luciferase reporter assay system, using a Lumat LB 9507 luminometer (Berthold Technologies, Bad Wildbad, Germany). The firefly luciferase activity, produced by PGL3-ArPII in identically treated triplicate samples, was normalized for the *Renilla* luciferase activity produced by phRL-CMV. The data shown are representative of at least three independent experiments. In the case of cotreatment with the NF-κB inhibitors, cells were preincubated for 2 h with CAPE (working concentration 20 μg/ml) or APDC (working concentration 100 ng/ml) and then incubated for 10 h with TGZ+LG. Another round of 2 h of CAPE plus 10 h of TGZ+LG was carried out before the cells were lysed for luciferase assay.

Western blotting

NIH-3T3 and KGN cells treated with either TGZ+LG or DMSO were grown to subconfluent phase, washed with PBS, and actively lysed in 500 μl lysis buffer. Samples were subjected to electrophoresis on 10% sodium dodecyl sulfate (SDS)-polyacrylamide gels and transferred onto nitrocellulose membranes. The membranes were incubated with either a rabbit polyclonal antibody against the p65 subunit of NF-κB [NF-κB p65 (c-20): sc-372, Santa Cruz Biotechnology, Santa Cruz, CA] or a rabbit polyclonal antibody against inhibitory κBα (IκBα) (c-21: sc-371, Santa Cruz Biotechnology) and subsequently with a horseradish peroxidase-linked goat antirabbit IgG secondary antibody (Cell Signaling Technology, Beverly, MA). Detection was carried out using the ECL+Plus Western blotting detection system (Amersham Biosciences, Buckinghamshire, UK). Membranes were then visualized using a STORM 860 scanner (Molecular Dynamics, Sunnyvale, CA). Images were finally analyzed using ImageQuant software (Molecular Dynamics).

ChIP assays

These were performed by the chromatin immunoprecipitation (ChIP) assay kit (Upstate Biotechnology, Lake Placid, NY), according to the protocol provided by manufacturer with some modifications. Briefly, KGN cells were seeded in 10-cm^2 dishes and treated overnight with 10 μM TGZ + 1 μM LG or the solvent DMSO. After an additional treatment of 10 ng/ml TNFα or its solvent normal saline (NS) for 1 h, cells were cross-linked with 1% formaldehyde for 60 min, washed with chilled PBS, resuspended in 200 μl SDS lysis buffer, and sonicated six times for 10

sec each at 60% maximum setting of the sonicator (Handy Sonic-UR-20P, TOMY SEIKO Co., Ltd., Tokyo, Japan). Sonicated cell supernatant was diluted 10-fold, and 1% (20 μl) of the total diluted lysate was used for total genomic DNA as input DNA control. The rest (1980 μl) was then subjected to immunoclearing by 75 μl salmon sperm DNA/protein A agarose-50% slurry for 30 min at 4 C. Immunoprecipitation was performed for overnight at 4 C with 3 μg p65 antibody (Santa Cruz Biotechnology). For negative control, normal rabbit IgG (Santa Cruz Biotechnology) was used instead of p65 antibody. Precipitates were washed sequentially for 5 min each in low salt, high salt, LiCH immune complex wash buffers, and finally washed twice with Tris/EDTA buffer. Histone complexes were then eluted from the antibody by freshly prepared elution buffer (1% SDS, 0.1 M $NaHCO_3$). Histone-DNA cross-links (including the input samples) were reversed by 5 M NaCl at 65 C for 4 h. DNA fragments were extracted with a PCR purification kit (Qiagen). One microliter from a 30-μl DNA extraction was used for PCR and primed by sequences as follows: forward, 5′-GGG AAG AAG ATT GCC TAA AC-3′; reverse, 5′-TGT GGA AAT CAA AGG GAC AG-3′; the PCR size was 401 bp.

Real-time PCR

Immunoprecipitated DNA samples were then set to real-time PCR analysis to quantify the relative amount to their corresponding input controls with a LightCycler (Roche Diagnostics GmbH, Mannheim, Germany) according to the manufacturer's instruction. Briefly, 1 μl immunoprecipitated DNA sample (or H_2O as negative control), was placed into a 20-μl reaction volume containing 1 μl of each primer (10 μM) and 2 μl LightCycler-FastStart DNA Master SYBR Green I (Roche), which includes nucleotides, Tag DNA polymerase, and buffer. PCR products were visualized on a 2% agarose gel and finally validated by direct sequencing. Input samples were amplified simultaneously as the internal controls. Real-time PCR data for each immunoprecipitated sample were calculated as a ratio to its corresponding input sample. Briefly, threshold values (crossing line) obtained where fluorescent intensity was in the geometric phase, cycle number at the crossing point of an immunoprecipitated sample (Cip), and the corresponding input sample (Cco) were determined via LightCycler software version 3.5. The relative amount to input sample of the immunoprecipitated sample (Aip) was calculated by the formula of: $Aip = 2^{(Cco-Cip)}$.

Statistics

One-way ANOVA followed by Scheffé's test was used for multigroup comparisons.

Results

TGZ+LG inhibited ArPII dose-dependently

We previously reported that TGZ+LG inhibit aromatase activity, and consistently the estrone production, in a dose-dependent manner (23). We also found that TGZ+LG down-regulated aromatase mRNA by both decreased transcription and increased degradation. Here a 4.0-kb fragment of human ArPII was inserted into PGL3-Basic to make the luciferase reporter PGL3-ArPII and then used to further address whether TGZ, LG, or TGZ+LG interfered with the transcription of aromatase from promoter II. KGN cells were transfected by Superfect with PGL3-ArPII as well as the internal control phRL-CMV. As shown in Fig. 1, on the addition of increasing concentration of TGZ+LG, the relative luciferase activity was decreased in a concentration-dependent manner. Although they were weaker, TGZ or LG alone also manifested inhibitory effects on ArPII. The results indicate that the inhibitory effect of TGZ+LG on aromatase gene is directly mediated by the inhibition of promoter II activity.

PPARγ is critical for the TGZ+LG inhibition

To further clarify the involvement of PPARγ in the regulation of ArPII, the same experiment as described above was carried out in NIH-3T3 cells, which lack endogenous expression of PPARγ (26). As shown in Fig. 2A, neither TGZ (or LG) alone nor combined treatment of TGZ+LG could decrease the expression of the PGL3-ArPII reporter, even when the concentration was raised to 10 μM for TGZ and 1.0 μM for LG, when the cells had been cotransfected with PGL3-ArPII+phRL-CMV and pcDNA3.1, the empty vector. However, on the exogenous cotransfection of the PPARγ expression vector, either TGZ or LG alone significantly decreased ArPII activity in a concentration-dependent manner, and combined treatment of TGZ+LG caused a sharper decrease in expression from the promoter. This phenomenon nicely mimicked what was observed in KGN cells, which possess endogenous PPARγ. These data clearly demonstrate the involvement of PPARγ in the inhibition of ArPII.

NF-κB inhibitors abolished the inhibition of TGZ+LG on aromatase gene

Due to the absence of a PPARγ-RXR-responsive element in the aromatase promoter II (23), we previously suggested that PPARγ might inhibit the promoter by an indirect mechanism (23). This hypothesis is supported by recent work (27), which showed that there was no binding of PPARγ and RXRα heterodimers to the promoter. A series of studies pointed out the inhibitory effect of PPARγ activation on NF-κB-dependent transcription system (28–30). We thus tested the possibility that PPARγ activation inhibits aromatase gene through the NF-κB system by using specific inhibitors for NF-κB: CAPE (31) and APDC (32). CAPE specifically inhibits NF-κB binding to DNA and also prevents the translocation of the p65 subunit of NF-κB to the nucleus and delays IκBα

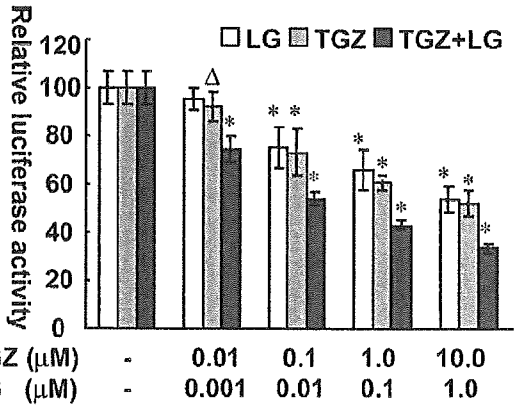

FIG. 1. TGZ+LG inhibits aromatase promoter II. The luciferase reporter PGL3-ArPII, wherein the luc+ gene is driven by a 4.0-kb segment of the human ArPII, was transfected into KGN cells, which were seeded in 12-well plates 1 d earlier. The cells were treated with an increasing concentration (as indicated) of TGZ, LG, or TGZ+LG 1 d after transfection for 24 h. Cells were then lysed and a dual-luciferase reporter assay was performed. The ArPII-mediated firefly luciferase signal was normalized using *Renilla* luciferase, which was constitutively expressed by the internal control phRL-CMV vector. Data expressed in mean ± SD was from identically treated triplicate samples of three independent experiments. Δ, $P < 0.05$; *, $P < 0.01$, compared with basal level of the same treatment group.

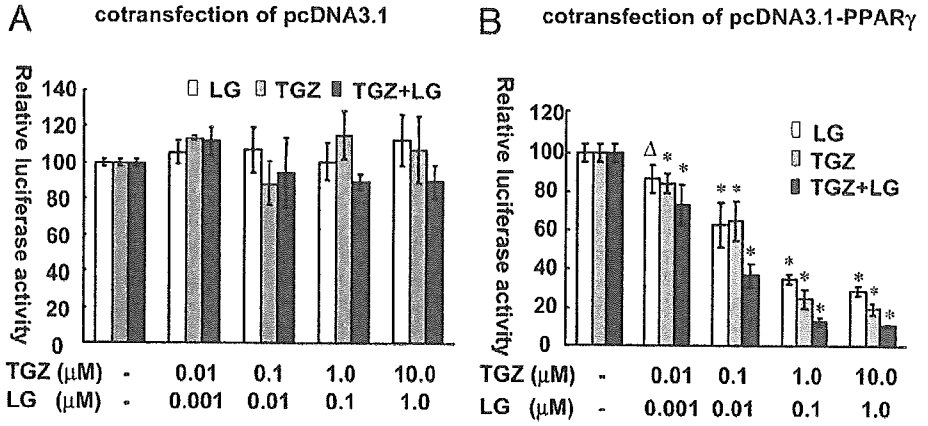

FIG. 2. TGZ+LG inhibits ArPII in a PPARγ-dependent manner. PPARγ-deficient NIH-3T3 cells were transfected with PGL3-ArPII; either a human PPARγ2 expression vector pcDNA3.1-PPARγ2 or the empty control pcDNA3.1 vector was cotransfected. Cells were then treated with TGZ, LG, or both for 24 h. Neither TGZ (or LG) alone nor TGZ+LG inhibited the promoter in the absence of PPARγ, whereas exogenous coexpression of the nuclear factor restored the inhibition. TGZ+LG synergistically inhibited the promoter in the presence of PPARγ. Δ, $P < 0.05$; *, $P < 0.01$, compared with basal level of the same treatment group.

resynthesis (31). As described above, cotransfection of PGL3-ArPII and pcDNA-PPARγ in NIH-3T3 cells allowed direct assessment of PPARγ mediation of the inhibitory effect on ArPII activity. CAPE was applied to this model to test the possible involvement of the NF-κB system in the inhibition. As shown in Fig. 3A, NIH-3T3 cells were treated with 20 μg/ml CAPE or 50% ethanol for 2 h before combined treatment with TGZ+LG, which lasted for 8 h. To gain a clearer inhibition, a second round of 2 h of CAPE plus 8 h of TGZ+LG was carried out before the cells were subjected to luciferase assay. Pretreatment of the cells with CAPE completely abolished the inhibitory effect of PPARγ activation, whereas the inhibition was still present with pretreatment with only the solvent for CAPE, 50% ethanol. A similar result was observed when CAPE was replaced by another NF-κB inhibitor, APDC (data not shown).

We next assessed whether the inhibition of aromatase activity caused by TGZ+LG also disappears on treatment with CAPE.

KGN cells were treated with CAPE in the same manner as above before aromatase activities were assayed. As shown in Fig. 3B, on pretreatment with 50% ethanol, the solvent for CAPE, TGZ+LG significantly inhibited aromatase activity, whereas once the cells were pretreated with CAPE, no decrease of aromatase activity was seen. These results indicate the mediation of NF-κB in the down-regulation of aromatase activity by TGZ+LG at the transcriptional level of promoter II.

NF-κB up-regulates ArPII

In the experiments described in Fig. 3, we noticed that on treatment of CAPE, even basal levels of both ArPII and aromatase activity were decreased, suggesting that NF-κB might be a positive regulator of aromatase gene. We tested this possibility by further experiments. As shown in Fig. 4A, cotransfection of the p65 subunit of NF-κB directly stimulated ArPII by 4-fold in NIH-3T3 cells. A similar phenomenon was observed in KGN cells (data not shown). NIK, which causes degradation of IκBα by phosphorylation of the latter at serine 176 and thus activates p65 (33), was used to specifically induce the endogenous activation of NF-κB. Figure 4B shows that PGL3-NF-κB, (positive control, contains three repeats of the NF-κB consensus elements) was augmented by NIK 2.80-fold. PGL-ArPII was also up-regulated 2.25 times by NIK. In the case of PGL3-Basic (negative control), NIK exhibited no effect.

TGZ+LG interfered with the interaction between NF-κB and ArPII

ChIP assay is a powerful technique to determine *in vivo* binding of transcription factors to target genes' promoters on

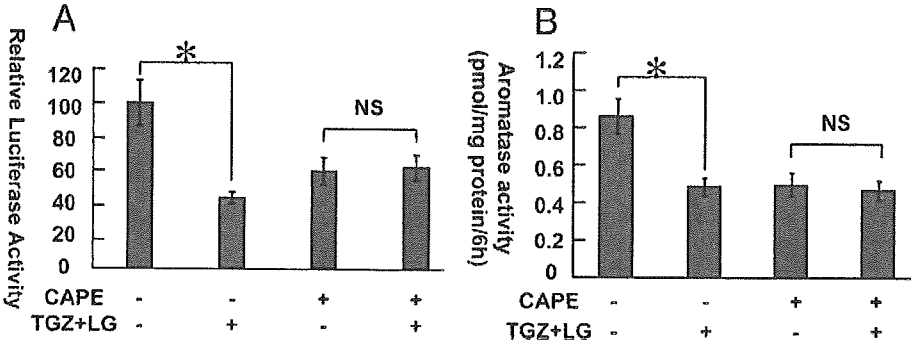

FIG. 3. TGZ+LG inhibition disappeared on NF-κB blockage. A, PGL3-ArPII was cotransfected with pcDNA3.1-PPARγ2 into NIH-3T3 cells. Cells were first treated with or without 20 μg/ml CAPE for 2 h and then with TGZ+LG or the solvent DMSO for 8 h. A second round of 2 h of CAPE (or the solvent 50% ethanol) and 8 h of TGZ+LG (or DMSO) treatment was carried out before cells were lysed for the luciferase assay. CAPE abolished the inhibitory effect of PPARγ activation and decreased the basal activity of the promoter as well. B, Aromatase activity assayed in KGN cells. Cells were treated with chemicals in the same manner as described in A. TGZ+LG inhibition of aromatase activity also disappeared on NF-κB blockage. *, $P < 0.01$; NS, not significantly different.

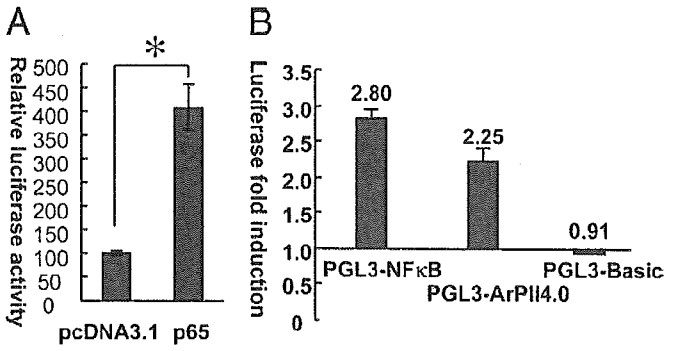

FIG. 4. NF-κB up-regulated ArPII. A, NIH-3T3 cells were transfected with PGL3-ArPII. pcDNA-p65 or pcDNA3.1 was cotransfected. ArPII activity was stimulated 4-fold by p65. B, pcDNA-NIK was transfected to NIH-3T3 cells to trigger the endogenous activation of NF-κB, whose effect on ArPII was evaluated by cotransfection of PGL3-ArPII. PGL3-NF-κB, a reporter containing three repeats of NF-κB elements, and PGL3-basic was also included as positive and negative controls, respectively. The *bars* represent the relative effect of NIK on each reporter; namely, the NIK-mediated reporter activity was divided by the control pcDNA3.1 empty vector-mediated reporter activity. *, $P < 0.01$.

chromatin. We used this assay to evaluate the interaction of NF-κB with ArPII, especially the recruitment of p65 to the promoter region. KGN cells pretreated either with an overnight 10 μM TGZ+1 μM LG or their solvent, DMSO, were challenged with 10 ng/ml TNFα or its solvent NS for 1 h before being subjected to ChIP assay with an antibody against p65. Enrichment of ArPII DNA sequences in the chromatin immunoprecipitates, which indicates association of p65 to the promoter within intact chromatin, was visualized by PCR amplification. Based on our primitive promoter deletion analysis data, which show that a 600-bp ArPII reporter already responds positively to p65 and NIK, we designed the PCR to amplify a 401-bp region of ArPII (−403 to −2, upstream of ovary exon 2, GenBank accession no. D21241). As shown in Fig. 5A, although a weak band was amplified (30 cycles) in the absence of antibody (lane 1, which may represent the nonspecific binding of the ArPII chromatin region to normal rabbit IgG), an increase in the relative intensity of ArPII PCR band amplified from samples treated with p65 antibody indicated binding between the transcription factor and the promoter (lanes 2–5). Among cells not pretreated with TGZ+LG, 1 h TNFα challenge seemed slightly increased band intensity (lane 3 *vs.* 2). Pretreatment of TGZ+LG clearly weakened the PCR band intensity (lane 4), suggesting a decreased occupancy by p65 on ArPII. However, the decrease was not observed in cells challenged with TNFα (lane 5). Control amplification was with total input DNA (Fig 5A, *lower panel*). There was no change in the amplification of input DNA in all cases.

To further objectively tell the difference between different groups of cells, we performed real-time PCR to quantify the relative amount of immunoprecipitated ArPII copies to input control for each sample. Figure 5B shows that presence of p65 antibody significantly increased the relative copy number of immunoprecipitated ArPII DNA segments, indicating that p65 associates with ArPII. And TGZ+LG pretreatment significantly reduced the relative copy number, suggesting the association was impaired. However, TNFα restored the TGZ+LG reduced relative ArPII copy number, although the cytokine did not change the copy number from cells not pretreated with TGZ+LG. Consistent with data presented in Fig. 4, these results indicated that NF-κB may interact with ArPII *in vivo*, and activation of PPARγ/RXR may interfere with the interaction.

The interference of PPARγ activation on the endogenous expression of NF-κB in KGN cells

The endogenous expression of the NF-κB system in KGN cells was tested by Western blotting, using antibodies against the p65 subunit and IκBα, and was positively controlled using NIH3T3 cells, whose endogenous NF-κB has already been proven (34). The KGN cells were treated with or without 24 h of 10 μM TGZ + 1.0 μM LG, actively lysed, and subjected to Western blotting. Figure 6 (*upper panel*) shows endogenous expression of IκBα in KGN cells and the *lower panel* the endogenous expression of the p65 subunit of NF-κB.

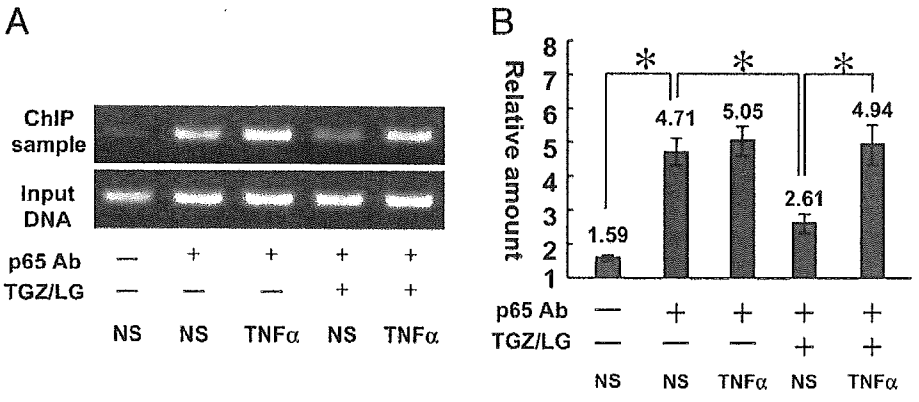

FIG. 5. ChIP assay of p65 binding to ArPII. KGN cells pretreated with or without an overnight 10.0 μM TGZ+1.0 μM LG were challenged with 10 ng/ml TNFα or its solvent, NS, for 1 h. ChIP assay was then performed with anti-p65 antibody or normal rabbit IgG as negative control. Enrichment of ArPII-specific DNA sequence in immunoprecipitated DNA pool indicating association of p65 with ArPII within intact chromatin was visualized by PCR. A, PCR was performed on immunoprecipitated DNA pool with normal rabbit IgG [p65 Ab (−)], p65 Ab, and purified input DNA (input). *Upper panel*, PCR amplified ArPII-specific bands from cells under various treatments as indicated. *Lower panel*, ArPII PCR bands from input controls. B, Real-time PCR was performed to quantify the amount of immunoprecipitated ArPII DNA copy number from cells under various treatments relative to their corresponding input controls. *, $P < 0.01$; NS, not significantly different.

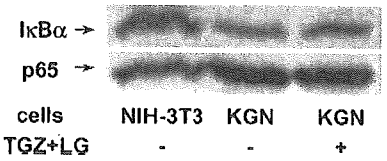

FIG. 6. TGZ+LG did not alter the endogenous expression of IκBα and p65. KGN cells were treated with 10.0 μM TGZ+1.0 μM LG for 24 h and were then subjected to Western blotting analysis for the IκBα and p65 subunits of NF-κB. NIH-3T3 cells were used as a positive control. KGN cells highly expressed both IκBα and p65, and 24 h of TGZ+LG did not apparently alter the protein expression levels.

Neither of these two proteins' expression was altered by a 24-h treatment of TGZ+LG, suggesting that PPARγ activation does not interfere with NF-κB function via down-regulation of p65 subunit expression or up-regulation of the IκB protein.

PPARγ activation suppresses NF-κB transactivation

As shown above, PPARγ activation does not apparently change the protein level of NF-κB but impairs the interaction between the transcription factor and ArPII. We subsequently studied the possible interference of PPARγ activation on NF-κB transactivation in KGN cells. As shown in Fig. 7, in KGN cells, cotransfection of 0.15 μg/well of pcDNA-p65 stimulated PGL3-NF-κB production (0.8 μg/well) approximately 4-fold, whereas the p65-augmented PGL3-NF-κB signal was decreased in a concentration-dependent manner on cotreatment with an increasing concentration of TGZ+LG. Thus, activation of PPARγ-RXR heterodimers by TGZ+LG resulted in inhibitory effects on NF-κB-mediated transcription. Namely, the final net outcome effect of PPARγ activation is a down-regulation of NF-κB transactivation activity.

Discussion

The physiological significance of the mysteriously high expression of PPARγ in ovarian granulosa cells is largely unknown. We previously reported that the synthetic PPARγ ligand, TGZ, in a concentration corresponding to human

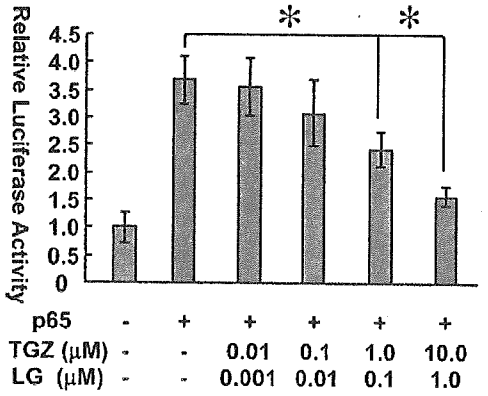

FIG. 7. TGZ+LG inhibited transactivation of NF-κB. KGN cells were transfected with PGL3-NF-κB, which contains three repeats of NF-κB elements. A p65 expression vector (pcDNA-p65) or the pcDNA3.1 empty vector was also transfected. Cells cotransfected with p65 were further treated with increasing concentrations of TGZ+LG for 24 h. TGZ+LG was shown to decrease p65-stimulated PGL3-NF-κB signal in a concentration-dependent pattern. *, $P < 0.01$.

plasma TGZ concentration after oral administration of a therapeutic dosage, caused a significant decrease in aromatase activity as well as mRNA level in human ovarian granulosa cells (21). The effect was enhanced synergistically by the specific ligand (LG) for RXR, the PPARγ partner. Consistently, TGZ+LG inhibited estrogen production in KGN cells (23), and TGZ reduced estrogen levels in patients with polycystic ovary syndrome, which suggested the *in vivo* relevance of the inhibition (35). In the present study, we further demonstrated that the aromatase promoter II, which is specially used in ovary, is also inhibited by TGZ+LG, indicating that inhibition occurs at the transcriptional level. It was recently reported that 15-deoxy-$\Delta^{12,14}$ prostaglandin J2, which is believed to be the endogenous ligand for PPARγ, inhibits aromatase activity through a PPARγ-independent, but redox-sensitive, mechanism (36). However, TGZ and LG, the synthetic ligands for PPARγ and RXR, respectively, seem to exert an inhibitory function in a PPARγ-dependent way because the inhibition of ArPII could not be observed in PPARγ-deficient NIH-3T3 cells unless the nuclear receptor is exogenously expressed. It is noteworthy that even for LG-induced inhibition, PPARγ was required, suggesting that inhibition requires PPARγ-RXR heterodimers. The important involvement of PPARγ in the regulation of the aromatase gene was also strengthened by a recent report that demonstrated that an environmental toxin, a commonly used plasticizer, di-C2-ethylhexyl phthalate, decreased aromatase expression through both PPARγ and PPARα in granulosa cells (37).

The aromatase gene is unique in that expression of the gene in different tissues is driven by different promoters in a tissue-specific pattern (8). Promoter II is typically used to drive the gene in ovarian granulosa cells, especially before menopause. Local estrogen production in breast adipose tissue has a definite mitogenic role in breast tumors (15, 16), and local estrogen levels in breast tumors were found 10 times higher than that in the circulation of postmenopausal women (38). Although in normal adipose tissue aromatase is mainly produced via the promoter I.4 (15, 39), the local accumulation of estrogen in breast adipose tissue containing a tumor is largely due to a critical shift in promoter usage from I.4 to II (12–14, 40). In this study, we found that TGZ+LG, in a PPARγ-dependent manner, dose-dependently inhibited ArPII activity in ovarian KGN cells as well as in fibroblast NIH-3T3 cells, suggesting that the PPARγ inhibitory effect on ArPII might be universal. These data highlighted the importance of ArPII and the therapeutic potency of TGZ+LG.

Due to the lack of an apparent consensus about PPARγ-responsive element on ArPII, we hypothesized that the inhibition mechanism might be indirect (23). This idea is supported by a recent study, which shows that PPARγ is unable to bind ArPII (27).

It has been proven that the ArPII gains its maximal activity when both PKA and protein kinase C are activated by cotreatment with forskolin and tetradecanoyl phorbol acetate (41, 42). NF-κB is one of the transcriptional factors that can be activated by the activation of the protein kinase C pathway (34). Whereas on the other hand, activation of PPARγ can regulate inflammatory responses by suppressing the activation of the transcriptional factor of NF-κB (28–30). In the

present study, we tested the hypothesis that PPARγ activation may exert its inhibitory effect on ArPII by inhibiting NF-κB, which is endogenously expressed in ovarian granulosa cells and breast tissues as well (43). In this study the inhibitory effect of PPARγ-RXR activation on both ArPII and aromatase activity was found to sharply disappear on treatment with NF-κB blockers (either CAPE or APDC), suggesting that NF-κB might be the mediator of this inhibition. If this is the case, NF-κB should logically be a positive regulator of ArPII. In line with this, the basal ArPII activity as well as the aromatase activity was decreased on CAPE treatment, and activation of the NF-κB system by either forced expression of p65 or cotransfection of NIK to activate endogenous NF-κB stimulated ArPII activity. Consistently, ChIP assay also showed the interaction between NF-κB and ArPII. However, no classical consensus NF-κB-responsive element was detected on the promoter. Nevertheless, because there is an instance that NF-κB may bind a DNA motif, which is not related to the classical NF-κB consensus sequence (44), we suppose that there might exist putative ArPII-specific binding sites for p65, which are to be further delineated.

Although we observed no effect of TGZ+LG on endogenous expressions of either IκBα or p65, which is considered one possible mechanism by which NF-κB system is regulated (45). Treatment of TGZ+LG apparently weakened the interaction between p65 and ArPII, suggesting activation of PPARγ may interfere with the formation of high-order complex between NF-κB and aromatase gene at chromatin level. This is probably further explained by the finding that activated PPARγ can physically interact with p65 and results in inhibition of NF-κB (46, 47). And probably as an outcome of the impaired transcription factor-promoter association, we found that PPARγ activation by TGZ+LG suppressed the transactivation ability of NF-κB. The suppression by the PPARγ-RXR nuclear receptor system may also possibly be related to the fact that the nuclear receptors compete for limited amounts of the general coactivators, cAMP response element-binding protein and steroid receptor coactivator-1, as we previously reported (48).

Considering our previous finding that activation of a PPARγ-RXR nuclear receptor system by TGZ+LG inhibits aromatase by accelerating mRNA degradation, we report in the present study that TGZ+LG inhibited transcriptional activity of the ArPII in a PPARγ-dependent manner. These data reinforce the potential use of synthetic PPARγ and RXR agonists for therapeutic applications in diseases in which estrogens, locally or systematically, play prominent pathogenic roles, especially in diseases like breast cancer. In addition, we found that the inhibition disappeared on blockage of NF-κB, which was found in turn to positively regulate aromatase. Notably, activation of NF-κB has been found involved in the proliferation and metastasis of breast cancer cells (43), for which, although several mechanisms have been suggested, we suppose that stimulation of aromatase might be an additional one. Classically, regulation of ArPII involves PKA-cAMP response element-binding protein (49) and the orphan nuclear receptor steroidogenic factor 1 (Ad4BP/SF-1) (50), but the actual regulation may be much more complicated, at least in that nuclear receptors like PPARγ, RXR, and their cross-talk with the transcriptional factor NF-κB might also play some important roles.

Acknowledgments

Received August 10, 2004. Accepted September 20, 2004.

Address all correspondence and requests for reprints to: Toshihiko Yanase, M.D., Ph.D., Department of Medicine and Bioregulatory Science, Graduate School of Medical Science, Kyushu University, Maidashi 3-1-1, Higashi-ku, Fukuoka 812-8582, Japan. E-mail: yanase@intmed3.med.kyushu-u.ac.jp.

References

1. **Thompson Jr EA, Siiteri PK** 1974 Utilization of oxygen and reduced nicotinamide adenine dinucleotide phosphate by human placental microsomes during aromatization of androstenedione. J Biol Chem 249:5364–5372
2. **Means GD, Kilgore MW, Mahendroo MS, Mendelson CR, Simpson ER** 1991 Tissue-specific promoters regulate aromatase cytochrome P450 gene expression in human ovary and fetal tissues. Mol Endocrinol 5:2005–2013
3. **Jenkins C, Michael D, Mahendroo M, Simpson E** 1993 Exon-specific northern analysis and rapid amplification of cDNA ends (RACE) reveal that the proximal promoter II (PII) is responsible for aromatase cytochrome P450 (*CYP19*) expression in human ovary. Mol Cell Endocrinol 97:R1–R6
4. **Tsai-Morris CH, Aquilana DR, Dufau ML** 1985 Cellular localization of rat testicular aromatase activity during development. Endocrinology 116:38–46
5. **Nitta H, Bunick D, Hess RA, Janulis L, Newton SC, Millette CF, Osawa Y, Shizuta Y, Toda K, Bahr JM** 1993 Germ cells of the mouse testis express aromatase. Endocrinology 132:1396–1401
6. **Naftolin F, Ryan KJ, Davies IJ, Reddy VV, Flores F, Petro Z, Kuhn M, White RJ, Takaoka Y, Wolin L** 1975 The formation of estrogens by central neuroendocrine tissues. Recent Prog Horm Res 31:295–319
7. **Roselli CE, Horton LE, Resko JA** 1985 Distribution and regulation of aromatase activity in the rat hypothalamus and limbic system. Endocrinology 117:2471–2477
8. **Simpson ER, Michael MD, Agarwal VR, Hinshelwood MM, Bulun SE, Zhao Y** 1997 Cytochromes P450 11: expression of the *CYP19* (aromatase) gene: an unusual case of alternative promoter usage. FASEB J 11:29–36
9. **Bokhman JV** 1983 Two pathogenetic types of endometrial carcinoma. Gynecol Oncol 15:10–17
10. **Sasano H, Harada N** 1998 Intratumoral aromatase in human breast, endometrial, and ovarian malignancies. Endocr Rev 19:593–607
11. **Yue W, Wang JP, Hamilton CJ, Demers LM, Santen RJ** 1998 *In situ* aromatization enhances breast tumor estradiol levels and cellular proliferation. Cancer Res 58:927–932
12. **Agarwal VR, Bulun SE, Leitch M, Rohrich R, Simpson ER** 1996 Use of alternative promoters to express the aromatase cytochrome P450 (*CYP19*) gene in breast adipose tissues of cancer-free and breast cancer patients. J Clin Endocrinol Metab 81:3843–3849
13. **Zhou C, Zhou D, Esteban J, Murai J, Siiteri PK, Wilczynski S, Chen S** 1996 Aromatase gene expression and its exon I usage in human breast tumors. J Steroid Biochem Mol Biol 59:163–171
14. **Harada N** 1997 Aberrant expression of aromatase in breast cancer tissues. J Steroid Biochem Mol Biol 61:175–184
15. **Bulun SE, Simpson ER** 1994 Competitive reverse transcription-polymerase chain reaction analysis indicates that levels of aromatase cytochrome P450 transcripts in adipose tissue of buttocks, thighs, and abdomen of women increase with advancing age. J Clin Endocrinol Metab 78:428–432
16. **Bulun SE, Price TM, Aitken J, Mahendroo MS, Simpson ER** 1993 A link between breast cancer and local estrogen biosynthesis suggested by quantification of breast adipose tissue aromatase cytochrome P450 transcripts using competitive polymerase chain reaction after reverse transcription. J Clin Endocrinol Metab 77:1622–1628
17. **Kliewer SA, Forman BM, Blumberg B, Ong ES, Borgmeyer U, Mangelsdorf DJ, Umesono K, Evans RM** 1994 Differential expression and activation of a family of murine peroxisome proliferator-activated receptors. Proc Natl Acad Sci USA 91:7355–7359
18. **Lemberger T, Desvergne B, Wahli W** 1996 PPARs: a nuclear receptor-signaling pathway in lipid metabolism. Annu Rev Cell Dev Biol 12:335–363
19. **Tontonoz P, Hu E, Graves RA, Budavari AI, Spiegelman BM** 1994 mPPAR γ2: tissue-specific regulator of an adipocyte enhancer. Genes Dev 8:1224–1234
20. **Braissant O, Foufelle F, Scotto C, Dauca M, Wahli W** 1996 Differential expression of peroxisome proliferator-activated receptors (PPARs): tissue distribution of PPAR-α, -β, and -γ in the adult rat. Endocrinology 137:354–366
21. **Mu YM, Yanase T, Nishi Y, Waseda N, Oda T, Tanaka A, Takayanagi R, Nawata H** 2000 Insulin sensitizer, troglitazone, directly inhibits aromatase activity in human ovarian granulosa cells. Biochem Biophys Res Commun 271:710–713
22. **Komar CM, Braissant O, Wahli W, Curry Jr TE** 2001 Expression and local-

ization of PPARs in the rat ovary during follicular development and the periovulatory period. Endocrinology 142:4831–4838
23. Mu YM, Yanase T, Nishi Y, Takayanagi R, Goto K, Nawata H 2001 Combined treatment with specific ligands for PPARγ:RXR nuclear receptor system markedly inhibits the expression of cytochrome aromatase in human granulosa cancer cells. Mol Cell Endocrinol 181:239–248
24. Yanase T, Mu YM, Nishi Y, Goto K, Nomura M, Okabe T, Takayanagi R, Nawata H 2001 Regulation of aromatase by nuclear receptors. J Steroid Biochem Mol Biol 79:187–192
25. Nishi Y, Yanase T, Mu Y, Oba K, Ichino I, Saito M, Nomura M, Mukasa C, Okabe T, Goto K, Takayanagi R, Kashimura Y, Haji M, Nawata H 2001 Establishment and characterization of a steroidogenic human granulosa-like tumor cell line, KGN, that expresses functional follicle-stimulating hormone receptor. Endocrinology 142:437–445
26. Tontonoz P, Hu E, Spiegelman BM 1994 Stimulation of adipogenesis in fibroblasts by PPAR γ 2, a lipid-activated transcription factor. Cell 79:1147–1156
27. Rubin GL, Duong JH, Clyne CD, Speed CJ, Murata Y, Gong C, Simpson ER 2003 Ligands for the peroxisomal proliferator-activated receptor γ and the retinoid X receptor inhibit aromatase cytochrome P450 (*CYP19*) expression mediated by promoter II in human breast adipose. Endocrinology 143:2863–2871
28. Wang N, Verna L, Chen NG, Chen J, Li H, Forman BM, Stemerman MB 2002 Constitutive activation of peroxisome proliferator-activated receptor suppresses pro-inflammatory adhesion molecules in human vascular endothelial cells. J Biol Chem 277:34176–34181
29. Ricote M, Li AC, Willson TM, Kelly CJ, Glass CK 1998 The peroxisome proliferator-activated receptor-γ is a negative regulator of macrophage activation. Nature 391:79–82
30. Jiang C, Ting AT, Seed B 1998 PPAR-γ agonists inhibit production of monocyte inflammatory cytokines. Nature 391:82–86
31. Natarajan K, Singh S, Burke Jr TR, Grunberger D, Aggarwal BB 1996 Caffeic acid phenethyl ester is a potent and specific inhibitor of activation of nuclear transcription factor NF-κB. Proc Natl Acad Sci USA 93:9090–9095
32. Fujii A, Harada T, Yamauchi N, Iwabe T, Nishi Y, Yanase T, Nawata H, Terakawa N 2003 Interleukin-8 gene and protein expression are up-regulated by interleukin-1β in normal human ovarian cells and a granulosa tumor cell line. Fertil Steril 79:151–157
33. Ozes ON, Mayo LD, Gustin JA, Pfeffer SR, Pfeffer LM, Donner DB 1999 NF-κB activation by tumor necrosis factor requires the Akt serine-threonine kinase. Nature 401:82–85
34. Diaz-Meco MT, Berra E, Municio MM, Sanz L, Lozano J, Dominguez I, Diaz-Golpe V, Lain de Lera MT, Alcami J, Paya CV 1993 A dominant negative protein kinase Cζ subspecies blocks NF-κB activation. Mol Cell Biol 13:4770–4775
35. Dunaif A, Scott D, Finegood D, Quintana B, Whitcomb R 1996 The insulin-sensitizing agent troglitazone improves metabolic and reproductive abnormalities in the polycystic ovary syndrome. J Clin Endocrinol Metab 81:3299–3306
36. Winnett G, van Hagen D, Schrey M 2003 Prostaglandin J2 metabolites inhibit aromatase activity by redox-sensitive mechanisms: potential implications for breast cancer therapy. Int J Cancer 103:600–605
37. Lovekamp-Swan T, Jetten AM, Davis BJ 2003 Dual activation of PPARα and PPARγ by mono-(2-ethylhexyl) phthalate in rat ovarian granulosa cells. Mol Cell Endocrinol 201:133–141
38. Van Landeghem AA, Poortman J, Nabuurs M, Thijssen JH 1985 Endogenous concentration and subcellular distribution of estrogens in normal and malignant human breast tissue. Cancer Res 45:2900–2906
39. Grodin JM, Siiteri PK, MacDonald PC 1973 Source of estrogen production in postmenopausal women. J Clin Endocrinol Metab 36:207–214
40. Bulun SE, Mahendroo MS, Simpson ER 1994 Aromatase gene expression in adipose tissue: relationship to breast cancer. J Steroid Biochem Mol Biol 49:319–326
41. Zhao Y, Agarwal VR, Mendelson CR, Simpson ER 1996 Estrogen biosynthesis proximal to a breast tumor is stimulated by PGE2 via cyclic AMP, leading to activation of promoter II of the *CYP19* (aromatase) gene. Endocrinology 137:5739–5742
42. Evans CT, Corbin CJ, Saunders CT, Merill JC, Simpson ER, Mendelson CR 1987 Regulation of estrogen biosynthesis in human adipose stromal cells. Effects of dibutyryl cyclic AMP, epidermal growth factor, and phorbol esters on the synthesis of aromatase cytochrome P-450. J Biol Chem 262:6914–6920
43. Watabe M, Hishikawa K, Takayanagi A, Shimizu N, Nakaki T 2004 Caffeic acid phenethyl ester induces apoptosis by inhibition of NFκB and activation of Fas in human breast cancer MCF-7 cells. J Biol Chem 279:6017–6026
44. Todorov VT, Volkl S, Muller M, Bohla A, Klar J, Kunz-Schughart LA, Hehlgans T, Kurtz A 2004 Tumor necrosis factor-α activates NFκB to inhibit renin transcription by targeting cAMP-responsive element. J Biol Chem 279:1458–1467
45. Delerive P, Gervois P, Fruchart JC, Staels B 2000 Induction of IκBα expression as a mechanism contributing to the anti-inflammatory activities of peroxisome proliferator-activated receptor-α activators. J Biol Chem 275:36703–36707
46. Chen F, Wang M, O'Connor JP, He M, Tripathi T, Harrison LE 2003 Phosphorylation of PPARγ via active ERK1/2 leads to its physical association with p65 and inhibition of NF-κβ. J Cell Biochem 90:732–744
47. Chung SW, Kang BY, Kim SH, Pak YK, Cho D, Trinchieri G, Kim TS 2000 Oxidized low density lipoprotein inhibits interleukin-12 production in lipopolysaccharide-activated mouse macrophages via direct interactions between peroxisome proliferator-activated receptor-γ and nuclear factor-κB. J Biol Chem 275:32681–32687
48. Uchimura K, Nakamuta M, Enjoji M, Irie T, Sugimoto R, Muta T, Iwamoto H, Nawata H 2001 Activation of retinoic X receptor and peroxisome proliferator-activated receptor-γ inhibits nitric oxide and tumor necrosis factor-α production in rat Kupffer cells. Hepatology 33:91–99
49. Michael MD, Michael LF, Simpson ER 1997 A CRE-like sequence that binds CREB and contributes to cAMP-dependent regulation of the proximal promoter of the human aromatase P450 (*CYP19*) gene. Mol Cell Endocrinol 134:147–156
50. Michael MD, Kilgore MW, Morohashi K, Simpson ER 1995 Ad4BP/SF-1 regulates cyclic AMP-induced transcription from the proximal promoter (PII) of the human aromatase P450 (*CYP19*) gene in the ovary. J Biol Chem 270:13561–13566

Endocrinology **is published monthly by The Endocrine Society (http://www.endo-society.org), the foremost professional society serving the endocrine community.**